



Universiteit  
Leiden  
The Netherlands

## Nanoparticle-based combination drug delivery systems for effective cancer treatment

He, Y.

### Citation

He, Y. (2024, June 25). *Nanoparticle-based combination drug delivery systems for effective cancer treatment*. Retrieved from <https://hdl.handle.net/1887/3765914>

Version: Publisher's Version

License: [Licence agreement concerning inclusion of doctoral thesis in the Institutional Repository of the University of Leiden](#)

Downloaded from: <https://hdl.handle.net/1887/3765914>

**Note:** To cite this publication please use the final published version (if applicable).

# Chapter 6

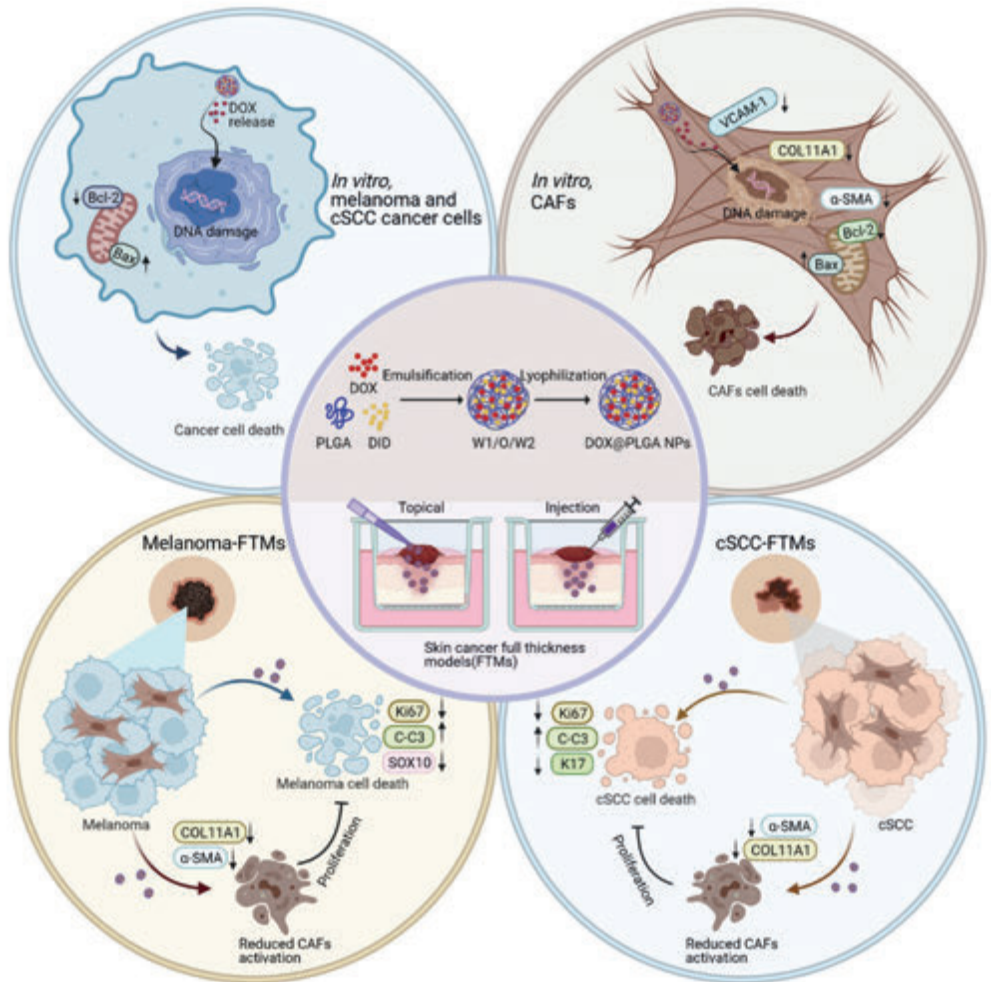
**Application of Doxorubicin-loaded PLGA NPs targeting both tumor cells and cancer-associated fibroblasts on human skin equivalents mimicking melanoma and cutaneous squamous cell carcinoma**

This chapter was adapted from “He, Y.; Wu, S.; Rietveld, M.; Vermeer, M.; Cruz, L.J.; Eich, C.; El Ghalbzouri, A. *Biomaterials Advances* 2024, 160, 213831”.

## Abstract

Nanoparticle (NP) use in cancer therapy is extensively studied in skin cancers. Cancer-associated fibroblasts (CAFs), a major tumor microenvironment (TME) component, promote cancer progression, making dual targeting of cancer cells and CAFs an effective therapy. However, dual NP-based targeting therapy on both tumor cells and CAFs is poorly investigated in skin cancers. Herein, we prepared and characterized doxorubicin-loaded PLGA NPs (DOX@PLGA NPs) and studied their anti-tumor effects on cutaneous melanoma (SKCM) (AN, M14) and cutaneous squamous cell carcinoma (cSCC) (MET1, MET2) cell lines in monolayer, as well as their impact on CAF deactivation. Then, we established 3D full thickness models (FTM) models of SKCM and cSCC using AN or MET2 cells on dermis matrix populated with CAFs respectively, and assessed the NPs' tumor penetration, tumor-killing ability, and CAF phenotype regulation through both topical administration and intradermal injection. The results show that, in monolayer, DOX@PLGA NPs inhibited cancer cell growth and induced apoptosis in a dose- and time-dependent manner, with a weaker effect on CAFs. DOX@PLGA NPs reduced CAF-marker expression and had successful anti-tumor effects in 3D skin cancer FTMs, with decreased tumor-load and invasion. DOX@PLGA NPs also showed great delivery potential in the FTMs and could be used as a platform for future functional study of NPs in skin cancers using human-derived skin equivalents. This study provides promising evidence for the potential of DOX@PLGA NPs in dual targeting therapy for SKCM and cSCC.

# Graphic Abstract





## 1 Introduction

Skin cancer is one of the most common cancer types worldwide in which the most prevalent forms include keratinocyte carcinomas, such as cutaneous squamous cell carcinoma (cSCC), and cutaneous melanoma (SKCM) [1]. SKCM is the most aggressive and fatal type of melanoma, with a poor prognosis if it becomes regionally invasive or metastatic. cSCC is a relatively less aggressive type of cancer compared to SKCM. However, it has a high annual incidence which may cause comparable numbers of deaths to SKCM [2]. In recent years, the perspective of cancer as a tumor cell-centered disease has shifted to the consensus of the interconnection and dependency of tumor microenvironment (TME). Cancer-associated fibroblasts (CAFs), as the predominant component of TME, have been widely reported to support tumor cell proliferation and invasion, as well as induce therapeutic resistance in various cancer types, including SKCM and SCCs [3]. For instance, CAFs were shown to increase Myla cell migration and reduce its sensitivity to Doxorubicin through *Cxcl12* secretion in Mycosis Fungoides [4]. In melanoma, CAFs can promote resistance to BRAF inhibition by producing a fibronectin-rich ECM [5]. Numerous studies suggested the benefits of targeting CAFs in help of suppressing tumor events, suggesting the promising trend in cancer therapy for dual targeting both cancer cells and CAFs [6].

Nanocarrier systems are widely used for drug delivery due to their tiny structure, improved drug stability, and adjusted drug release kinetics [7]. Poly (lactic-co-glycolic acid) (PLGA) is a copolymer that consists of lactic acid and glycolic acid (50:50) [8]. It has been approved by the U.S. Food and Drug Administration and the European Medicines Agency for use as a drug delivery system in humans due to its biocompatibility, biodegradability, and non-toxicity [9,10]. Numerous studies have suggested the potential of PLGA NPs in delivering chemotherapeutic agents for favor cancer-targeting [11]. However, the use of PLGA NPs in CAF-targeting therapy is yet to be explored. Moreover, among the chemotherapeutics loaded in nanocarrier systems, doxorubicin (DOX) is one of the most frequently chosen options as it not only harms cancer cells but also induces immunogenic cell death (ICD) which results in eliciting antitumor immunity [12]. Utilization of PLGA NPs has been demonstrated to effectively control the release of DOX, thereby reducing its cytotoxicity and minimizing the previously reported side effects. To date, the effect of DOX@PLGA NPs on CAFs has not been thoroughly studied.

Considering the high cost and limited availability of human trials, as well as the distinct differences in structure and properties between animal skin and human skin [13,14], alternative methods are needed to investigate dermal drug

delivery. To closely mimic the characteristics of native and diseased human skin, a reconstructed 3D human skin equivalent (HSE) has been established and extensively utilized in a wide range of skin-related studies, especially for accessing the toxicity and efficacy of therapeutic agents [15]. Moreover, the establishment of a 3D tumorous full-thickness model (FTM), an advanced type of HSE in which a stratified tumor epidermis is formed on top of a dermal matrix containing CAFs, allows for the observation of drug penetration and its effects on tumor-stroma interaction. This model allows for the simultaneous evaluation of drug efficacy on both tumor cells and the TME, providing a more comprehensive understanding of drug response.

This study aimed to investigate the impact of PLGA NPs loaded with DOX (DOX@PLGA NPs) on both tumor cells and CAFs. The NPs were prepared using a double emulsion solvent evaporation method, and their anti-proliferative and pro-apoptotic effects, as well as their cellular uptake, were evaluated in monolayer cultures. Subsequently, 3D organotypic cultures were established to mimic SKCM and cSCC and the NPs were applied topically or via intradermal injection to gain insights into the potential use of DOX@PLGA NPs in treating skin cancers by targeting both tumor cells and the TME.

## **2 Materials and Methods**

### **2.1 Chemicals and reagents**

Fetal bovine serum (FBS), dulbecco's modified eagle's medium (DMEM), ham's F12 medium (F12), and collagenase were purchased from Gibco Laboratories (Thermo Scientific™, Waltham, MA, USA). PLGA polymer (Mw=17,000 g/mol) was provided by Caribion PURAC (Amsterdam, Netherlands). Polyvinyl alcohol (PVA) (Mw 13–23 kg/mol, 87–89% hydrolyzed), ascorbic acid, dispase II, cell proliferation reagent WST-1 (cat. No. 11644807001), and chloroform (CHCl<sub>3</sub>, Mw 119.38 g/mol) were acquired from Sigma Aldrich (Merck, Darmstadt, Germany). Trypsin and penicillin-streptomycin (P/S, 10,000 U/mL), 4',6-diamidino-2-phenylindole, dilactate (DAPI), 1,1'-dioctadecyl-3,3',3'-tetramethylindodicarbocyanine (DiD), and alexa fluor™ 488 phalloidin were provided by Thermo Fisher Scientific (Waltham, Massachusetts, USA). DOX (Mw 579.98 g/mol, 98.0–102.0% (HPLC)) was acquired from Euroasia Co., Ltd. (Delhi, India). The formula of all culture medium used in this study are listed as follow: F5 medium: DMEM+ 5% FBS + 1% P/S. K5 medium: DMEM/F12 (at 3:1 ratio) + 5% FBS + 1% P/S + 1.1 μM hydrocortisone

+ 1  $\mu\text{M}$  isoproterenol + 0.087  $\mu\text{M}$  insulin (Sigma-Aldrich). K0 medium: DMEM/ Ham's F12 medium (at a 3:1 ratio) + 1% P/S + 0.55  $\mu\text{M}$  hydrocortisone + 1  $\mu\text{M}$  isoproterenol + 0.087  $\mu\text{M}$  insulin + 10 mM L-serine + 50.6 nM selenious acid + 10  $\mu\text{M}$  L-carnitine (Sigma-Aldrich).

## 2.2 Preparation of NPs

As previously reported [16–19], NPs were prepared using an oil-in-water ( $W_1/O/W_2$ ) double-emulsion solvent evaporation technique. Briefly, 30 mg of PLGA was dissolved in 3 mL of chloroform at room temperature (RT) for 3 min, while 3 mg of DOX was dissolved in 300  $\mu\text{L}$  of ultrapure water. These solutions were mixed and thoroughly emulsified using a probe sonicator (Sonifier 250, Branson, Danbury, USA) to form a primary emulsion ( $W_1/O$ ) at a drug-PLGA ratio of 1:10 (w/w). 20 mL of 2% PVA was thoroughly mixed and re-emulsified with the primary emulsion to form a double emulsion with the aid of a probe sonicator. The resulting emulsion was stirred on a magnetic stirrer for 3 h at RT to fully evaporate the chloroform. After being washed 3 times with ultrapure water, the NPs were freeze-dried. To calculate the reaction yields of the produced NPs by the following formula:

Equation 1

$$\text{Reaction Yield (\%)} = \frac{\text{Actual Yield}}{\text{the initial amount of reactants used in the reaction}} \times 100\%$$

## 2.3 Characterization of NPs

The zeta potential, polydispersity index (PDI), and average size of the NPs were measured using the Malvern ZetaSizer 2000 (Malvern, Worcestershire, UK), as described previously [17,20]. First, the freeze-dried NPs were redispersed into deionized water (100  $\mu\text{g}/\text{mL}$ ). The NPs were then well dispersed through gentle sonication, and subsequently, the NPs were measured using dynamic light scattering. The nanoparticle properties were analyzed using ZetaSizer.

## 2.4 Transmission electron microscopy (TEM)

The shape and morphology of the NPs were determined by transmission electron microscopy (TEM). A 20  $\mu\text{L}$  solution of 1 mg/mL NPs was uniformly applied to a

200 mesh copper grid (Ted Pella Inc., Redding, CA, USA) and after 1 min, excess sample was blotted off with filter paper and stained with 10  $\mu$ L of 2% uranyl acetate for 1 min. The NP samples were then air dried at RT for 10 min. TEM images were acquired and stored using a Tecnai 12 Twin (FEI, Oregon, USA) at 120 kV.

## 2.5 Encapsulation efficiency and drug loading

To determine the encapsulation efficiency and drug loading of DOX, 3 mg of NPs were dissolved in 0.5 mL of dimethylformamide (DMF, Thermo Scientific™, Waltham, MA, USA) for 12 h to induce complete degradation of the PLGA matrix and release of DOX from the NPs. The PLGA debris was then removed by centrifugation at 14.9  $\times$ g for 20 min. After centrifugation, the supernatant was collected and the DOX concentration was assessed at 480 nm using a SpectraMax® iD3 multi-mode microplate reader (Marshall Scientific, Hampton, USA). The drug loading (Equation 3) and encapsulation rates (Equation 2) of DOX in NPs were calculated as follows:

Equation 2

$$\text{Encapsulation rate (\%)} = \frac{\text{the amount of drug released from lyophilized PLGA NPs}}{\text{the amount of drug originally used to prepare NPs}} \times 100\%$$

Equation 3

$$\text{Drug loading (\%)} = \frac{\text{amount of drug found in lyophilized NPs}}{\text{amount of lyophilized NPs}} \times 100\%$$

## 2.6 *In vitro* Drug Release

The *in vitro* release kinetics of DOX from NPs was studied in PBS at different pHs (pH 5.0, 6.5 and 7.4). 5 mg of NPs (DOX amount equal to 50  $\mu$ g) were dissolved in dialysis bags (MWCO 3500) containing pH 5.0, pH 6.5 and pH 7.4 PBS, respectively, and then the bags were placed in tubes containing the corresponding pH of PBS and stirred continuously at 100 rpm for 30 days in a shaker incubator at 37°C. 1 mL of sample solution was taken in triplicate at the indicated time points. The release of DOX was measured at 480 nm using a SpectraMax M3 multi-mode microplate reader. The drug release experiment was repeated three times for each time point and averaged.

## 2.7 Stability of NPs

As previously described [21], 3 mg of NPs were dissolved in 15 mL of medium containing 10% FBS or 50% FBS, respectively, and stored at 37°C at 150 rpm for 7 days. 1mL sample was removed from the NPs mixture each day. The mean diameter of the NPs and the change in zeta potential were then measured by Malvern ZetaSizer 2000.

## 2.8 2D cell culture

CAFs were isolated from cSCC tumor biopsies supplied by the Department of Dermatology (LUMC, the Netherlands). After removing the horny layers, hairs and excess normal skin, tumor biopsies were cut into small pieces and incubated in Collagenase / Dispase II at 37°C for 2 h. Then the cells were filtered through a 70 µm cell strainer, cultured in F5 medium and used within Passage 5.

Human melanoma cell line AN (skin metastasis) was kindly provided by H. Randolph Byers (Harvard Medical School, Boston, USA) and the M14 cell line (lymph node metastasis) was kindly provided by Kenneth L. Scott (Dana Farber Cancer Institute, Boston, USA). Two cell lines were both cultured in F5 medium at 37°C with 5% CO<sub>2</sub>.

cSCC cell lines MET1 (invasive) and MET2 (recurrent) were kindly provided by Professor C. Proby (Division of Cancer Research, Medical Research Institute, Jacqui Wood Cancer Centre Ninewell Hospital & Medical School, Dundee). Both cell lines were cultured in K5 medium supplemented with 2 ng/mL epidermal growth factor (EGF) at 37°C and 7.3% CO<sub>2</sub>.

## 2.9 Cell viability assays

AN, M14, MET1 and MET2 were seeded in 96-well plates at a density of 3000 cells/well one day prior to refreshment of corresponding culture medium containing a range of concentrations of NPs at 1.8, 3.6, 7.2, 14.4, 28.8, 57.6 µg PLGA/mL (DOX equivalent concentration of 0.125, 0.25, 0.5, 1, 2, 4 µg/mL). CAFs were seeded the same way but treated with NPs in a different gradient of concentrations at 7.5, 15, 30, 60, 120, 240, 480 µg PLGA/mL (DOX equivalent concentration of 0.5, 1, 2, 4, 8, 16 µg/mL). Cell viability was detected after 24 h and 48 h of NP treatment using the WST-1 kit according to the manufacturer's instruction. After 1h incubation at 37°C

in the dark, the absorbance in each well was measured at a wavelength of 450 nm by a Thermo Scientific Microplate Reader (Thermo Fisher, USA).

## 2.10 Apoptosis assays

CAFs ( $1 \times 10^4$  cells/well), AN ( $1 \times 10^4$  cells/well), M14 ( $1 \times 10^4$  cells/well), MET1 ( $1 \times 10^4$  cells/well) and MET2 ( $1 \times 10^4$  cells/well) cells were inoculated in 24-well plates. After 24 h incubation, tumor cells were incubated with the concentration of 12.3  $\mu\text{g/mL}$  NPs (DOX equivalent concentration at 0.8  $\mu\text{g/mL}$ ) while CAFs were treated with 61.5  $\mu\text{g/mL}$  NPs (DOX equivalent concentration at 4  $\mu\text{g/mL}$ ) for 24 and 48 h of incubation. Next, cells were collected and stained with membrane linked protein V/FITC and 7AAD (both from Sigma Aldrich, Sigma Aldrich, Darmstadt, Germany) for 20 min at RT. A total of 10,000 events were analyzed using a FACS Calibur instrument (Beckton-Dickson, LSR III, Bioscience, N.J., USA) and the percentage of cells in different apoptotic states was analyzed by FlowJo software v10.0.

## 2.11 Western blotting

Protein samples from each cell type cultured with or without NPs were collected using Radioimmunoprecipitation assay (RIPA) buffer containing protease and phosphatase inhibitors. The corresponding protein concentration was determined using Pierce™ BCA Protein Assay Kit according to the manufacturer's instructions. Next, Samples were diluted 1:3 with loading buffer and heated in a heat plate at 95°C for 5 min. Proteins were separated on SDS-PAGE and transferred to PVDF membranes (polyvinylidene difluoride membranes). Primary antibodies including anti-bcl-2 (#68103-1-Ig, 1:1000, Proteintech), anti-bax (60267-1-Ig, 1:1000, Proteintech), anti- $\alpha$ -SMA (#61001, 1:500, Progen), and anti- $\beta$ -actin (#81115-1-RR, 1:1000, Proteintech) were then incubated overnight at 4°C. Next day, membranes were washed 3 times with PBST buffer, followed by a 90 min incubation with IRDye™ 800 fluorescently labelled secondary antibody at RT. Finally the protein bands were visualized in an Odyssey® XF imaging system. Quantification of the protein expression was performed in Image J (National Institutes of Health, USA).

## 2.12 NP cellular uptake

Uptake of NPs by CAFs, AN, M14, MET1 and MET2 cells was analyzed by flow

cytometry (Beckton-Dickson, LSR III, Bioscience, N.J, USA) and confocal laser scanning microscopy (CLSM, Leica TCS SP8 X, Germany). For flow cytometry, CAFs ( $1 \times 10^4$  cells/well), AN ( $1 \times 10^4$  cells/well), M14 ( $1 \times 10^4$  cells/well), MET1 ( $1 \times 10^4$  cells/well) and MET2 cells ( $1 \times 10^4$  cells/well) were seeded in 24-well plates, followed by 12.3  $\mu\text{g}/\text{mL}$  PLGA NP incubation for 1, 4, 24, and 48 h. Plates were washed with cold PBS to stop the cellular uptake and to remove the redundant NPs. Then, cells were harvested and resuspended in FACS buffer. Finally, the fluorescence intensity of individual cells was quantified using a flow cytometer (10,000 total events/reading). For CLSM, CAFs ( $1 \times 10^3$  cells/well), AN ( $1 \times 10^3$  cells/well), M14 ( $1 \times 10^3$  cells/well), MET1 ( $1 \times 10^3$  cells/well) and MET2 cells ( $1 \times 10^3$  cells/well) were seeded on top of culture slides (Nutagon) and cultured at 37°C in 5% CO<sub>2</sub> for 24 h prior to the incubation with 12.3  $\mu\text{g}/\text{mL}$  PLGA NPs for 1, 2, 4, 24 and 48 h. After treatment, cells were washed 3 times with pre-cooled PBS, fixed with 4% (w/v) paraformaldehyde (PFA) for 15 min at RT, washed twice with PBS, and stained with FITC phalloidin for 40 min at 37°C. Next, nuclei were stained with DAPI for 3 min at RT. Finally, the samples were imaged by a confocal microscope (Leica DM5500 B, Leica Microsystem CMS GmbH, Mannheim, Germany) using a 100x objective.

### 2.13 Quantitative real-time PCR analysis (qRT-PCR)

CAFs were seeded in 6-well plates and treated with NPs for 48 h at the concentration of 61.5  $\mu\text{g}/\text{mL}$  (corresponding DOX concentration is 4  $\mu\text{g}/\text{mL}$ ). At the endpoint of the treatment, Total RNA was extracted by using Favorprep total RNA purification mini kit (FATRK001-2) according to the manufacturer's protocol. The extracted total RNA was reverse transcribed into complementary DNA using the iScript cDNA synthesis kit (BioRad, Veenendaal, The Netherlands). qRT-PCR was performed using IQ SYBR Green Supermix (BioRad) on a CFX384 system (BioRad). All primers were synthesized by Sigma-Aldrich and the sequences were listed in Supplementary Table 1.

### 2.14 3D organotypic culture & NP application

3D FTMs mimicking SKCM and cSCC were established by seeding AN and MET2 cells onto the dermal matrix populated with CAFs respectively. Briefly,  $4 \times 10^4$  CAFs were seeded in the pre-made rat-tail collagen and cultured for a week with F5 medium, followed by seeding  $7.5 \times 10^4$  AN or MET2 cells on top. FTMs were incubated for two days under submerged condition at 37°C with 7.3% CO<sub>2</sub> in K5

medium. Thereafter, the culture medium was supplemented with 12  $\mu\text{M}$  BSA, 5  $\mu\text{M}$   $\beta$ -dextrine, 10  $\mu\text{M}$  L-carnitine, 10 mM L-serine, 50 nM selenious acid, 250  $\mu\text{M}$  L-ascorbic acid phosphate, 1  $\mu\text{M}$  DL- $\alpha$ -tocopherol, 7  $\mu\text{M}$  ara-chidonic acid, 15  $\mu\text{M}$  linoleic acid and 25  $\mu\text{M}$  palmitic acid (all from Sigma-Aldrich) while the concentration of FBS was reduced to 1% and the hydrocortisone to 0.55  $\mu\text{M}$ . Next, FTMs were cultured at the air-liquid interface for two weeks using the same culture medium without FBS and an increased concentration of linoleic acid to 30  $\mu\text{M}$  until harvest. For NP treatment, FTMs were divided into 10 groups: negative control group, topical control group (10% glycerin/PBS), PLGA NP topical day 2 group, PLGA NP topical day 4 group, PLGA NP injection day 2 group, PLGA NP injection day 4 group, DOX@PLGA NP topical day 2 group, DOX@PLGA NP topical day 4 group, DOX@PLGA NP injection day 2 group and DOX@PLGA NP injection day 4 group. For topical treatment, 61.5  $\mu\text{g}/\text{mL}$  NPs (equivalent DOX con. at 4  $\mu\text{g}/\text{mL}$ ) were dissolved in 100  $\mu\text{l}$  10% glycerin/PBS and applied daily on top of the surface of each FTM for 4 h. For injection, NPs at the same concentration were dissolved in 100  $\mu\text{L}$  DMEM and evenly injected in the dermis at 4 different spots once in 2 days using a 1mL syringe.

### **2.15 Hematoxylin and eosin (H&E) staining & immunohistochemical (IHC ) staining**

One part of each FTM was fixed in 4% paraformaldehyde, dehydrated and paraffin embedded. Histological analysis was performed on 4  $\mu\text{m}$  sections by hematoxylin and eosin (H&E) staining. For IHC staining, 4  $\mu\text{m}$  sections were deparaffinized, rehydrated, and sent for antigen retrieval. After blocking in 2% Normal Human Serum (NHS) for 20 min, sections were incubated overnight with various primary antibodies at 4°C (Ki67, #M7240, DAKO, 1:100; K17, #M7046, DAKO, 1:25; Cleaved Caspase-3, #9661, CST, 1:750; SOX10, #EP268, CELL MARQUE, 1:100), and labelled using the streptavidin-biotin-peroxidase system (GE Healthcare), according to the manufacturer's instruction. Finally, all slides were counterstained with hematoxylin and mounted with Kaiser's glycerin.

### **2.16 Quantification of relative epidermal thickness**

Representative pictures of H&E staining performed on each FTMs were loaded in Image J software. The whole FTM can be separated into three areas: (A) tumor epidermis, (B) invaded tumor areas in the dermis and (C) the whole dermal matrix. Within the program, boundaries were manually set for each compartment

to calculate the corresponding area. The relative tumor thickness equals the percentage of whole tumor compartment area in each corresponding FTM (A+B/A+B+C%) when compared to the control group. Results were presented as the mean  $\pm$  SD of six counts in three different donors.

### 2.17 Immunofluorescence (IF) staining

For 2D cell culture, CAFs were seeded on glass culture slides (Nutagon) at a density of  $1 \times 10^3$  cells/well and cultured at 37°C with 5% CO<sub>2</sub> for 24 h before the treatment with PLGA NPs and DOX@PLGA NPs for 48 h. Then, slides were fixed in 4% paraformaldehyde at RT, followed by incubation with 0.1% Triton X-100 (v/v in PBS) for 10 min. Next, cells were blocked in 2% NHS for 30 min at RT prior to the incubation with primary antibodies including COL11A1 (GeneTex, #GTX55142, 1:200) and VCAM-1 (abcam, #ab134047, 1:250) at 4°C overnight. Then cells were incubated with alexa 488- labeled secondary antibody (Invitrogen, 1:250) at RT for an 1 h, followed by 5 min staining of DAPI, and finally mounted with anti-fade mounting medium (H-1000, VECTASHIELD). For FTMs, 4  $\mu$ m sections were processed in the same way as in IHC staining until the primary antibody ( $\alpha$ -SMA, #61001, Progen, 1:250; pro-COL11A1, #CI0011, Oncomatrix, 1:125) incubation step. Then slides were incubated with Cy3-labelled secondary antibody for 1 h at RT, (Jackson immunoresearch, 1:500) and counterstained with DAPI for 5 min afterwards. Finally, all slides were mounted using H-1000 anti-fade mounting medium and stored at 4°C.

### 2.18 Distribution of NPs in FTMs

One part of each FTMs was snap-frozen in liquid nitrogen and stored in -80°C. 5  $\mu$ m frozen sections were cut using a thermostatic frozen sectioning machine at -15°C to -20°C and then mounted with VECTASHIELD (H-1200, Vector Laboratories, Burlingame, CA). The fluorescence images were visualized using Leica AF6000 (Leica AF6000, Leica, Wetzlar, Germany).

### 2.19 Statistical analyses

Statistical analyses were completed in GraphPad Prism software version 8.0.1 (CA, USA). Dual comparisons were made with an unpaired Student's *t*-test. Two-way analysis of variance (ANOVA) was used for multi-group comparisons. Experimental

data were expressed as mean  $\pm$  standard deviation (SD). In all comparisons, a  $p$ -value  $\leq 0.05$  was considered to be significantly different.

### 3 Results

#### 3.1 Preparation and characterization of NPs

To prepare DOX-loaded NPs, we utilized the high water solubility of DOX and the high lipid solubility of DID to efficiently encapsulate them in a biodegradable PLGA via the Water-in-Oil-in-Water ( $W_1/O/W_2$ ) double emulsion technique, resulting in the synthesis of DOX@PLGA NPs (Fig. 1A). The morphology of the NPs was confirmed by TEM. As shown in Figure 1B, both DOX@PLGA NPs and blank PLGA NPs exhibited a similar smooth spherical structure on the surface. The particle size, zeta potential, and PDI of the NPs were measured using the ZetaSizer. As shown in Figure 1C, the average particle sizes of PLGA NPs and DOX@PLGA NPs were  $195.3 \pm 2.77$  nm and  $178.3 \pm 1.96$  nm, respectively. Additionally, the surface charges were  $-8.26 \pm 0.62$  mV and  $-6.56 \pm 0.42$  mV for PLGA NPs and DOX@PLGA NPs, respectively, indicating that the NPs were uniformly distributed in size. Overall, DOX was successfully loaded into the PLGA NPs without altering their physicochemical properties. Calculated from Equation 1, the reaction yield of the generated NPs is about 23.72%. Previous studies have reported that the concentration of serum proteins can impact the stability and particle size of NP solutions [22]. Next, we determined the stability of the NPs by measuring the size (Fig. 1D) and zeta potential (Fig. 1E) of NPs in DMEM containing 10% and 50% FBS for 30 days. The results showed that the average particle size of NPs in DMEM with 50% FBS increased by approximately 5–7 nm relative to that in DMEM with 10% FBS. This demonstrates that NPs maintained a reasonable size even in higher concentrations of serum, which is more conducive to the delivery of chemotherapeutic drugs to tumor sites. No significant differences were observed in the aforementioned parameters after 30 days in varying concentrations of FBS, indicating the promising stability of our NPs.

Given that blood transport and endocytosis are the primary processes involved in the uptake and transport of NPs [23], NPs undergo transport from early endosomes (pH 6.5) to lysosomes (pH 5.0) during the endocytosis process. Therefore, we investigated the cumulative release of DOX from DOX@PLGA NPs under simulated conditions of physiological pH (pH 7.4), early endosomes (pH 6.5), and lysosomes (pH 5.0), respectively [24]. At 24 h, the release of DOX was 59.6% (pH 7.4), 71.1%

(pH 6.5), and 82.2% (pH 5.0), respectively (Fig. 1F). At 48 h, 89.4% of DOX was released from a pH 5.0 solution. As the pH was increased to early endosomal (pH 6.5) and physiological (pH 7.4) pH values, the release of DOX decreased correspondingly (dropping to 79.6% and 67.8% at 48 h timepoint respectively) (Fig. 1F). This indicates that, at the same time point, the lower the pH value, the higher the cumulative release of DOX. After 8 days, drug release reached a plateau and remained stable. Approximately 97.7% of DOX was released after 30 days in pH 5.0, while 89.2% and 75.1% of DOX were present in solutions at pH 6.5 and 7.4, respectively (Fig. 1G). In conclusion, over the 30-day release period, the release rate of DOX at pH 7.4 was the slowest, followed by pH 6.5, and the release rate was the fastest at pH 5.0.

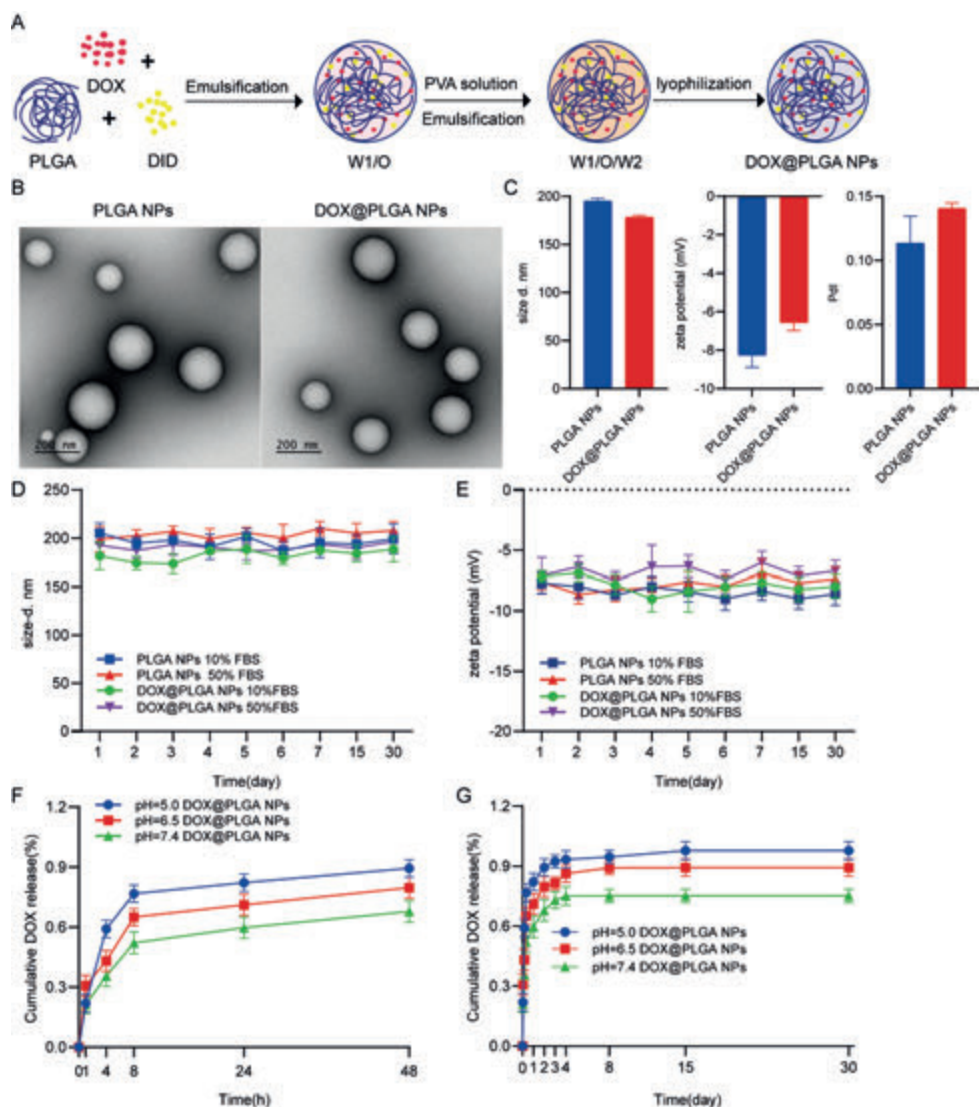


**Figure 1.** The synthesis and physicochemical characterization of NPs. (A) The synthetic route of DOX@PLGA NPs. (B) TEM images of PLGA NPs and DOX@PLGA NPs using 2% (w/v) phosphotungstic acid negative staining. (C) The size, zeta potential, and PDI of NPs in PBS were determined using DLS. Colloidal stability analysis of NP (D) size and (E) zeta potential in cell culture medium containing 10% FBS and 50% FBS for 7 days. Cumulative release of DOX@PLGA NPs over time in PBS at pH 5.0, 6.5 and 7.4 after (F) 48 h and (G) 30 days. Data was presented as mean  $\pm$  SD from 3 independent experiments. \*  $p < 0.05$ .

### 3.2 Cytotoxic effects of DOX-loaded PLGA NPs on SKCM and cSCC tumor cell lines

To assess the cytotoxicity of PLGA NPs and DOX@PLGA NPs on human SKCM (AN, M14) and cSCC (MET1, MET2) cells, we treated tumor cell lines with different concentrations of DOX@PLGA NPs (0, 1.8, 3.6, 7.2, 14.4, 28.8 and 57.6  $\mu\text{g}/\text{mL}$  PLGA) for 24 h and 48 h. We observed a significant time- and concentration-dependent anti-proliferative effect of DOX@PLGA NPs on all four tumor cell lines. In contrast, the corresponding concentrations of blank PLGA NPs showed little toxicity. The  $\text{IC}_{50}$  of DOX@PLGA NPs was calculated for AN, M14, MET1 and MET2 cells. The data showed that at 48 h, an average of approximately 12.3  $\mu\text{g}/\text{mL}$  DOX@PLGA NPs (corresponding DOX concentration of 0.8  $\mu\text{g}/\text{mL}$ ) reduced cell growth by 50% in M14, MET1 and MET2 cells, while half of that concentration was already sufficient for AN cells (Fig. 2, A–D).

To further analyze the effect of NPs on apoptosis in SKCM (AN, M14) and cSCC (MET1, MET2) cells, Annexin V-FITC/7AAD staining (Fig. 2E–2H) and western blot (Fig. 2I–2J) were performed. Based on the  $\text{IC}_{50}$  results of NPs from all tumor cell lines, NPs were chosen for further apoptosis analysis at a concentration of 12.3  $\mu\text{g}/\text{mL}$ . To this end, we first examined the pro-apoptotic effect of DOX@PLGA NPs on AN, M14, MET1 and MET2 cells using flow cytometry. As shown in Figure 2E–2H, blank PLGA NPs did not induce significant apoptosis compared to the control group, whereas the percentages of apoptotic cells increased to 38.25%, 42.60%, 49.1% and 61.33% in AN, M14, MET1 and MET2 cells, respectively, after treatment with DOX@PLGA NPs for 24 h. After 48 h treatment, the percentage of cells undergoing apoptosis further increased to 62.65%, 62.91%, 69.25% and 84.78% in AN, M14, MET1 and MET2 cells, respectively. Then, the expression of apoptosis-related proteins, including Bax and Bcl-2, was analyzed by Western blot (Fig. 2I–2J). Within the Bcl-2 family, Bax initiates the caspase cascade, thereby inducing apoptosis in cells, while Bcl-2, as a competitor for Bax, possesses anti-apoptotic activities [25]. The expression of Bcl-2 and Bax showed no significant difference after PLGA NPs treatment compared to the control group. In contrast, the expression level of Bcl-2 was down-regulated in the DOX@PLGA NPs group ( $p < 0.05$ ), while Bax expression was merely changed, resulting in a decrease in the Bcl-2/Bax expression ratio. Therefore, based on the above results, DOX@PLGA NPs significantly elevated apoptosis in all four tumor cell lines compared to the corresponding control group by regulating the protein expression of Bcl-2 family members. (Fig. 2I–2J).

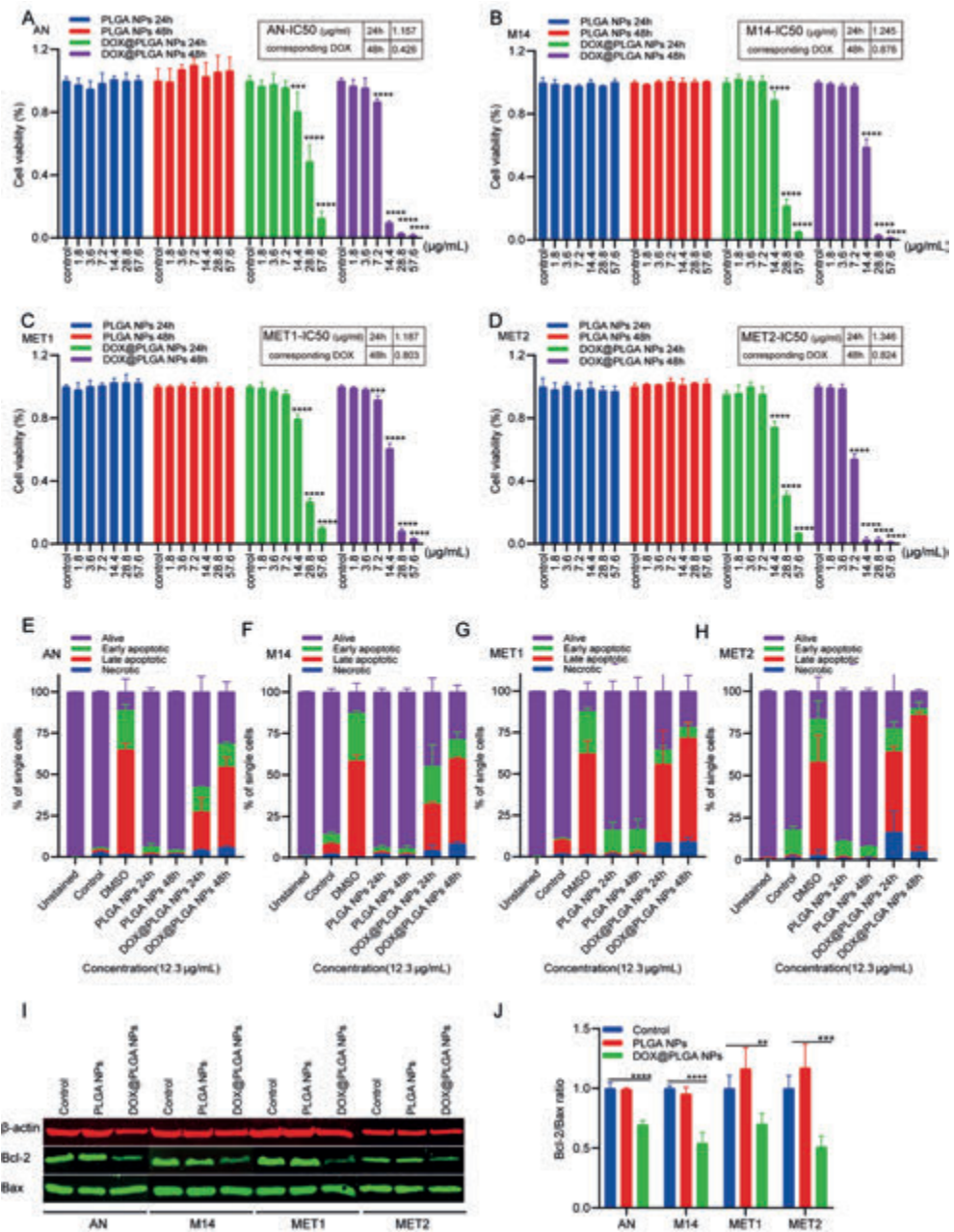


**Figure 2.** The anti-proliferative and pro-apoptotic effect of DOX@PLGA NPs in SKCM and cSCC cell lines. The cell viability of (A) AN, (B) M14, (C) MET1, and (D) MET2 cells was measured by WST-1 assays after treatment with or without various concentrations of blank PLGA NPs or DOX@PLGA NPs for 24 h and 48 h. Annexin V/ 7-AAD staining was performed to measure the apoptosis of (E) AN,

(F) M14, (G) MET1, and (H) MET2 cells after 24 and 48 h treatment with or without PLGA NPs and DOX@PLGA NPs. (I) Protein expression of Bcl-2 and Bax in AN, M14, MET1 and MET2 treated with or without PLGA NPs and DOX@PLGA NPs for 48 h was detected by western Blotting,  $\beta$ -actin was used as the internal control. (J) Quantification of the expression ratio of Bcl-2/Bax in each cell type. Data was presented as mean  $\pm$  SD from 3 independent experiments. \*\*  $p < 0.01$ , \*\*\*  $p < 0.001$  and \*\*\*\*  $p < 0.0001$ .

### 3.3 DOX@PLGA NPs de-activated CAFs

Based on the promising anti-tumor effect of DOX@PLGA NPs, we further explored whether it could regulate CAFs. First, by treating CAFs with a concentration range of DOX@PLGA NPs (7.5, 15, 30, 60, 120, 240, 480  $\mu$ g/mL PLGA), we observed that DOX@PLGA NPs gradually inhibited CAFs cell viability with increased concentrations and prolonged NP incubation times, while blank PLGA NPs did not affect CAFs cell growth at corresponding concentrations (Fig. 3A). The  $IC_{50}$  of DOX@PLGA NPs on CAFs for 24 h and 48 h treatment were 228.165  $\mu$ g/mL (equivalent DOX con. at 14.84  $\mu$ g/mL) and 52.398  $\mu$ g/mL (equivalent DOX con. at 3.408  $\mu$ g/mL), respectively, which were much higher than the corresponding  $IC_{50}$  of DOX@PLGA NPs in tumor cells as mentioned earlier. Furthermore, a huge increase in the fraction of apoptotic CAFs (51.04%) in the DOX@PLGA NP-treated group was noticed compared to the control and PLGA NP groups (both below 10%) after 24 h. Later on, prolonged CAFs culture with DOX@PLGA NPs for 48 h increased the percentage of CAFs undergoing apoptosis to 68.02% (Fig. 3B). The apoptosis status was also validated at protein level (Fig. 3C). The expression of Bcl-2 in DOX@PLGA NP-treated CAFs was significantly decreased while Bax expression showed little change compared to the control and PLGA NP-treated group, leading to a decrease in the expression ratio of Bcl-2/Bax (Fig. 3D), which indicated the onset of apoptosis in CAFs. Additionally, we found that DOX@PLGA NPs also regulated the expression of several CAFs markers and effectors, including  $\alpha$ -SMA, COL11A1 and VCAM-1, which have been proven to be crucial for CAFs biology and tumor cell-CAF crosstalk [26–28]. qPCR data revealed that, despite no obvious effect being observed on the expression of the aforementioned markers in PLGA NP-treated CAFs, DOX@PLGA NPs significantly reduced the mRNA expression of  $\alpha$ -SMA (\*  $p < 0.05$ , Fig. 3F), COL11A1 (\*\*  $p < 0.01$ , Fig. 3G) and VCAM-1 (\*  $p < 0.01$ , Fig. 3H). Immunoblotting results further validated the downregulation of  $\alpha$ -SMA after DOX@PLGA NP treatment compared to control and blank PLGA NP groups (Fig. 3C, 3E). Similarly, immunofluorescence staining showed a significant reduction in the expression intensity of COL11A1 (Fig. 3I) and

VCAM-1 (Fig. 3J) after treatment with DOX@PLGA NPs. Taken together, DOX@PLGA NPs inhibited CAFs cell viability, induced apoptosis, and deactivated CAFs by reducing the expression of their markers and effectors.

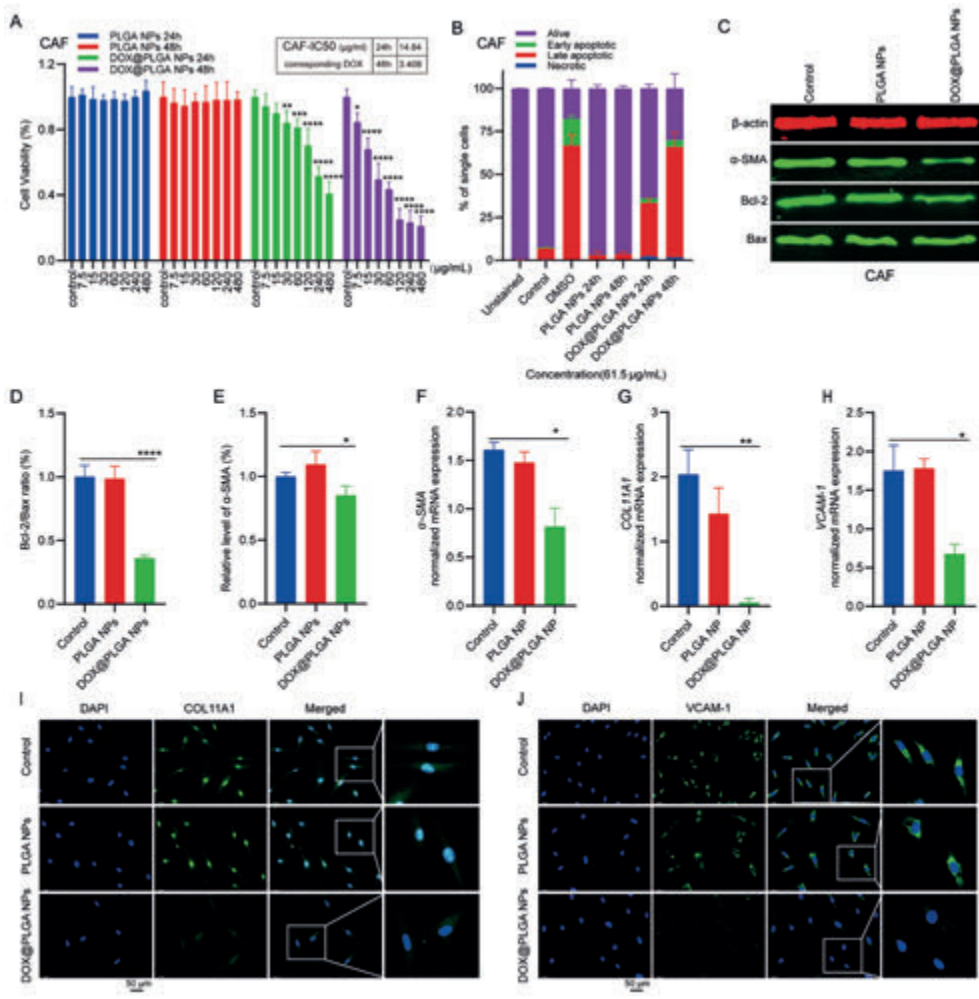


**Figure 3.** The effect of DOX@PLGA NPs on CAFs cell viability, apoptosis and activation. (A) CAFs were treated with or without various concentrations of PLGA NPs and DOX@PLGA NPs for 24 h and 48 h followed by the cell viability detection by using WST-1 assays. (B) Apoptosis rate of CAFs after treated with or without PLGA NPs and DOX@PLGA NPs. (C) Protein expression of  $\alpha$ -SMA, Bcl-2 and Bax in CAFs treated with or without PLGA NPs and DOX@PLGA NPs.  $\beta$ -actin was used as the internal control. (D) Quantification of the protein expression ratio of Bcl-2/Bax. (E) quantification of the protein expression of  $\alpha$ -SMA. By qPCR, the mRNA

expression of (F)  $\alpha$ -SMA, (G) COL11A1, (H) VCAM-1 in CAFs treated with or without PLGA NPs and DOX@PLGA NPs was detected. By immunofluorescence staining, the protein expression of (I) COL11A1 (green) and (J) VCAM-1 (green) in CAFs treated with or without PLGA NPs and DPX@PLGA NPs was determined. Scale bar = 50  $\mu$ m. Data was presented as mean  $\pm$  SD from 3 independent experiments. \*  $p < 0.05$ , \*\*  $p < 0.01$ , \*\*\*  $p < 0.001$  and \*\*\*\*  $p < 0.0001$ .

### 3.4. *In vitro* cellular uptake of NPs

The uptake efficiency of our DID-labeled PLGA NPs were measured in AN, M14, MET1, MET2, and CAFs at a series of time points up 48 h using flow cytometry and CLSM. According to the data from the flow cytometry analysis, the average fluorescence intensity (AFI) of DID fluorescence was negligible at 0h and 1h. Starting from 4 h, the AFI of PLGA NPs began to enhance, and dramatically augmented at 24 h. Finally, we observed a peak of NP uptake at 48 h, indicating a time-dependent increase in NP uptake in all cell types (Fig. 4A, 4B). Similarly, using CLSM, a minimal DID-positive signal was detected at 1h, whereas from the 4 h incubation onwards, we observed a gradual increase in dotted fluorescence signals moving from the edge of the cytoplasm towards the nuclei in CAFs (Fig. 4C), AN (Fig. 4D), M14 (Fig. 4E), MET1 (Fig. 4F) and MET2 cells (Fig. 4G). In addition, we compared the uptake capacity of NPs by different cell types at the same time point (Supplementary Figure 1), and found that cSCC cell lines (MET1 and MET2) showed a rapid NP uptake compared to SKCM cell lines (AN and M14) and CAFs before 4 h, whereas after 24 h, an obvious acceleration of NP uptake speed was noticed in M14 cells and CAFs. In general at the endpoint, MET2 cells showed the greatest uptake capacity of NPs, followed by M14, CAFs and AN, while MET1 demonstrated the least.

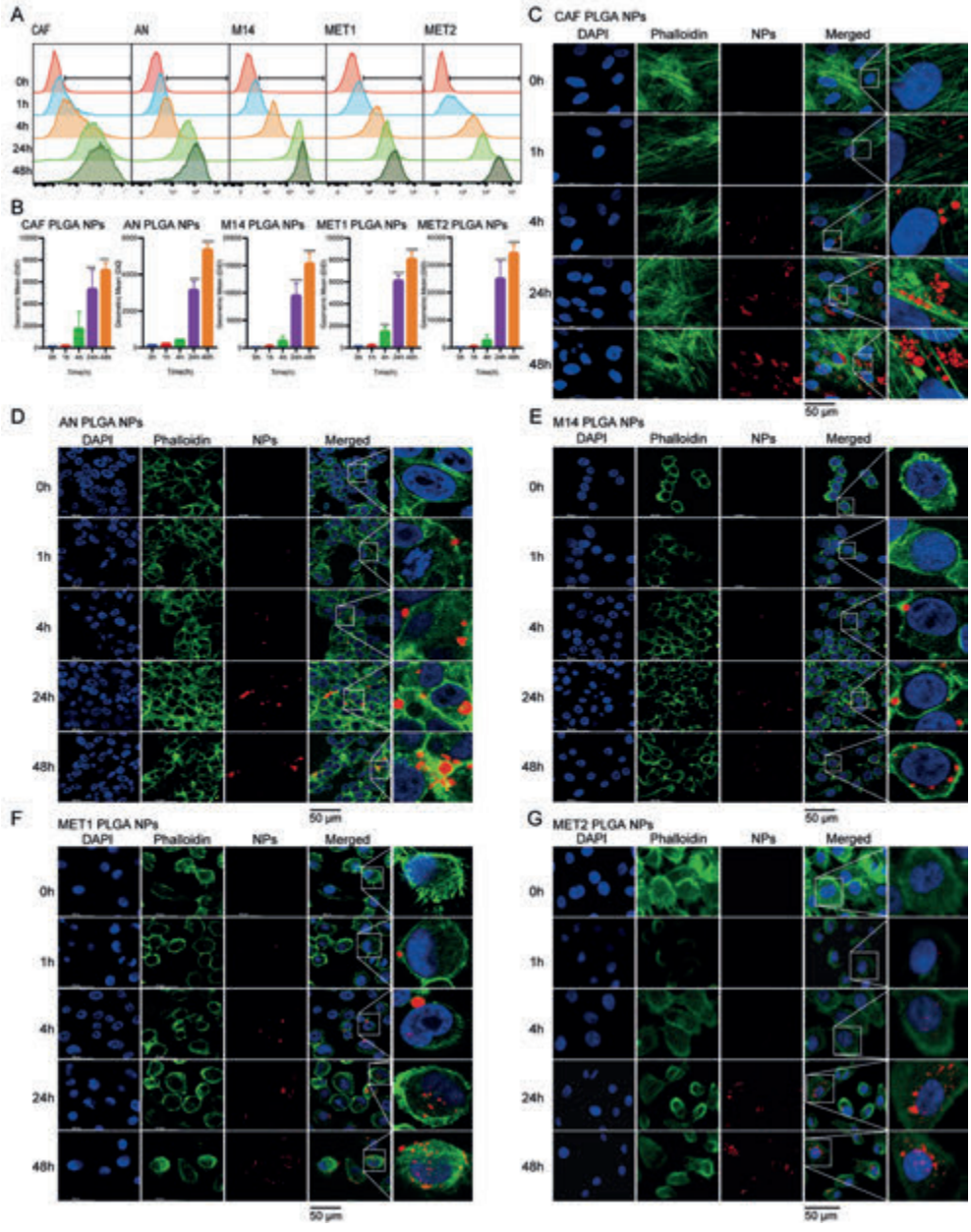


**Figure 4.** NP uptake ability of AN, M14, MET1, MET2 and CAFs cells. All cell types were treated with or without PLGA NPs for 0, 1, 4, 24 and 48 h. (A) Representative flow cytograms of the take-in of DID-labelled NPs in all cell types. (B) Geometric mean of flow cytometric analysis of fluorescence intensity in all cell types. Images of (C) CAFs, (D) AN, (E) M14, (F) MET1 and (G) MET2 cells absorbing NPs were acquired from CLSM. Nuclei was stained with DAPI (blue), actin filaments on cell

membranes were stained with Phalloidin (green), and DID-labelled NPs were visualized in red. Scale bar = 50  $\mu\text{m}$ . Data was presented as mean  $\pm$  SD from 3 independent experiments. \*\*\*  $p < 0.001$  and \*\*\*\*  $p < 0.0001$ .

### 3.5 The applicability of NPs in SKCM and cSCC FTMs

To meet the translational purposes, we established 3D organotypic cultures mimicking SKCM and cSCC, and further explored the applicability of DOX@PLGA NPs in these 3D tumorous models by topical treatment or intradermal injection. Figure 5A illustrates the work flow of FTM establishment and NP application. In brief, SKCM (AN) and cSCC (MET2) cells were seeded on the dermal matrix populated with CAFs and cultured under the air/liquid surface. NP treatment was initiated on day 22. Herein, due to the stratification of tumor cells yielding a stronger and more resistant tumor epidermis in the 3D models, as well as the support of the dermal compartment, we treated the FTMs with a concentration of NPs equal to 5 times  $IC_{50}$  on the tumor cells (61.5  $\mu\text{g}/\text{mL}$ ) calculated in 2D culture, in combination with our previous experience of drug screening on 3D FTMs. For topical treatment, to facilitate better penetration of NPs through the skin epidermis, 61.5  $\mu\text{g}/\text{mL}$  PLGA NPs or DOX@PLGA NPs (equivalent DOX con. at 4  $\mu\text{g}/\text{mL}$ ) were dissolved in 100  $\mu\text{L}$  10% glycerin/PBS and mixed to prepare the NP solution. The solution was then applied uniformly on top of the surface of each FTM for 4 h per day. The application was repeated daily for a total of 2 or 4 days. For injection, NPs at the same concentration were dissolved in 100  $\mu\text{L}$  DMEM and injected from 4 different spots through the surface to the dermis in each FTM once in 2 days for 2 days or 4 days till termination. As circled by red lines in the macroscopic pictures, both administrations reduced the thickness of tumor epidermis in AN-FTMs (Fig. 5B) and MET2-FTMs (Fig. 5C) compared to the corresponding negative and topical control groups. Since DID fluorescence is rather stably retained in NPs, it was used as a tracer for tracking the NP distribution in FTMs. As shown in Figure 5D and 5E, the majority of NP accumulation was found in the tumor epidermis while occasional epidermal-to-dermal penetration was also noticed in the topical treatment group. In contrast, the fluorescent signals of NPs were mainly scattered around in the dermal compartment of FTMs administered by NP injection. Histological analyses showed that 3D co-culturing AN or MET2 cells with CAFs led to the formation of a stratified tumor epidermis and invasive tumor islands in the dermis. Either topical application or injection of blank PLGA NPs to AN-or MET2 FTMs showed scarcely any toxicity whereas DOX@PLGA NPs treatment by both administration methods significantly thinned the tumor epidermis and cleared the invaded tumor areas on a time-dependent manner in AN-FTMs (Fig. 5F, 5G) and MET2-FTMs (Fig. 5H, 5I).

However little difference was found between the two application means within the same treatment period. These results suggest that NPs can be successfully applied to deliver DOX in 3D skin tumor models via different administration routes, and that DOX@PLGA NPs effectively inhibited the proliferation and migration of both SKCM and cSCC cells in FTMs.

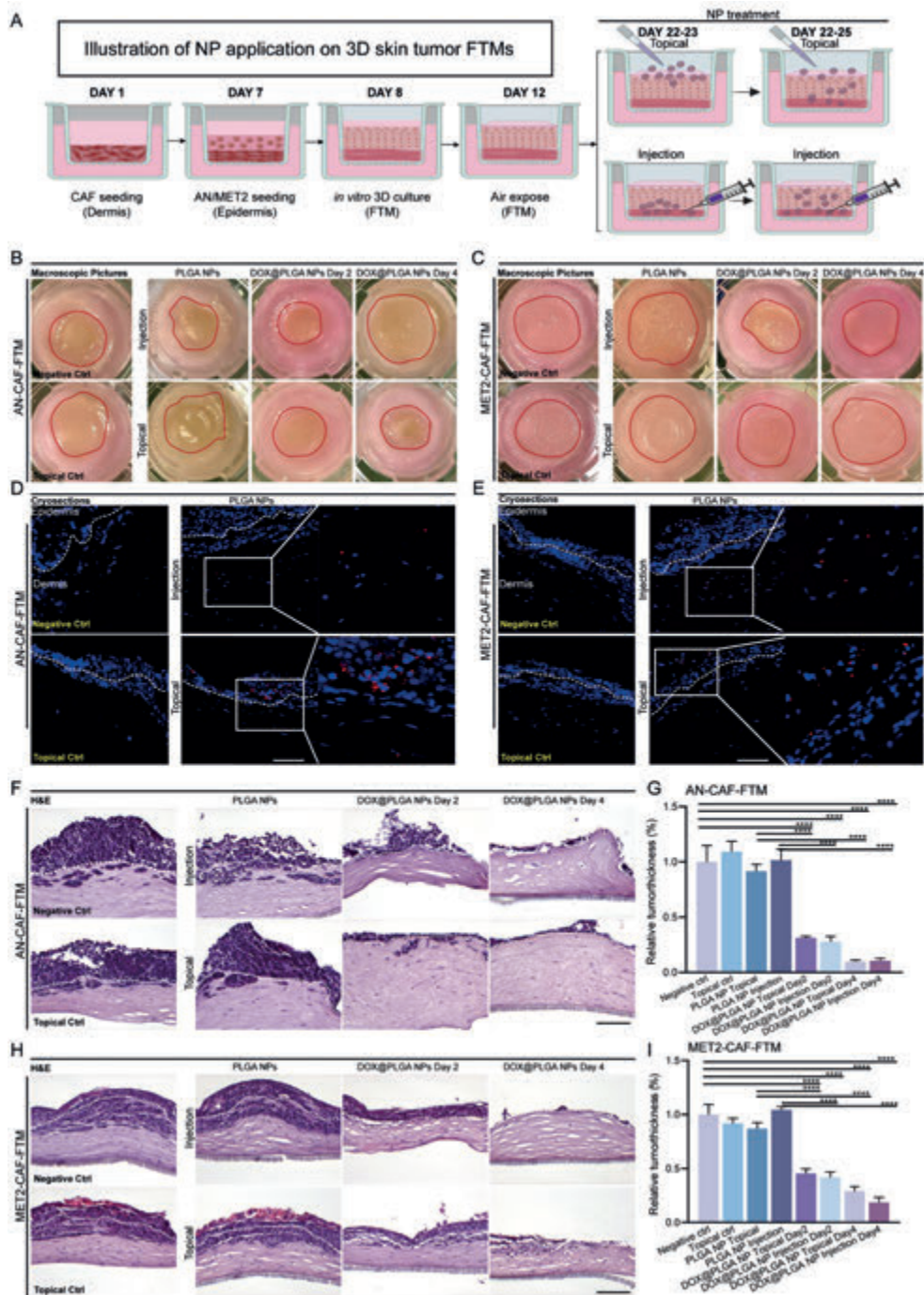


**Figure 5.** The application and effect of NPs on AN- and MET2-FTMs. (A) Schematic representation of the experimental timeline for NP treatment on FTMs.

Macroscopic images of (B) AN-FTMs and (C) MET2-FTMs treated with or without PLGA NPs and DOX@PLGA NPs were presented. The distribution of PLGA NPs in (D) AN-FTMs and (E) MET-FTMs treated with or without PLGA NPs was followed with a fluorescence microscope. Cell nuclei were stained blue with DAPI and the DID-labelled PLGA NPs were red. Histological observations were collected from H&E staining on (F) AN-FTMs and (H) MET2-FTMs treated with or without PLGA NPs and DOX@PLGA NPs. Quantification of Relative Tumor Thickness (% of negative control) was calculated in (G) AN-FTMs and (I) MET2-FTMs. Scale bar = 100  $\mu$ m. Data was presented as mean  $\pm$  SD from 3 independent experiments. \*\*\*\*  $p < 0.0001$ .

### **3.6 DOX@PLGA NPs inhibited tumor cell proliferation and invasion in SKCM and cSCC FTMs**

Next, we examined the effect of DOX@PLGA NPs on tumor cell proliferation and apoptosis by IHC staining of Ki67 and Cleaved Caspase 3 (C-C3), respectively, in both AN- and MET2-FTMs. As shown in Figure 6A and B, Ki67 positive cells were distributed throughout the entire tumor epidermis as well as the invaded dermal tumor parts in control AN-FTMs. The application of control PLGA NPs, either topically or by injection, did not affect tumor cell proliferation whereas 2 days of DOX@PLGA NP treatment by both administrations significantly decreased the presence of Ki67+ cells within the tumor epidermis. Prolonged treatment with DOX@PLGA NPs resulted in a more pronounced elimination of proliferating tumor cells, indicating a strengthened anti-proliferative effect by 4 days of NP application. No clear difference was found in effectiveness between topical application and injection in AN-FTMs. Similar results were obtained from MET2-FTMs (Fig. 6C and D), where Ki67+ cells mainly resided in the invasive tumor areas in control and blank PLGA NP treated groups. With prolonged DOX@PLGA NP treatment, more reduction of Ki67+ cells was observed. In addition, topical application of DOX@PLGA NPs was more effective than NP application by injection, especially in day 4 treatment groups. C-C3 is used as a marker of cell death due to its ability to hydrolyze the majority of the proteins involved in the apoptotic process [29]. In this study, scarcely any positive staining was found in control and PLGA-NP-treated tumor FTMs (Fig. 6E, F, G, H). In contrast, topical application of DOX@PLGA NP significantly induced the percentage of apoptotic tumor cells in a time-dependent manner. Two days of DOX@PLGA NP injection also increased the proportion of apoptotic cells albeit with no statistically significant difference compared to control and PLGA-NP-treated group. Enhanced pro-apoptotic effect of DOX@PLGA NP was only observed in 4-day injection groups.

In the next step, we assessed the effect of DOX@PLGA NPs on the expression of markers which closely correlate with SKCM and cSCC progression, respectively. For instance, SOX10 is a differentiation-sensitive marker of melanoma that is associated with a fast proliferative and highly invasive state of melanoma cells [30,31]. Keratin 17 (K17) expression is a major basis for the diagnosis of SCCs and positively regulates SCC cell activation [32]. By IHC staining, as shown in Figure 6 I, AN cells in the control groups abundantly expressed SOX10. There was no difference in SOX10 expression in FTMs treated with PLGA NPs compared to the controls. However, the expression of SOX10 was significantly decreased in AN-FTM after DOX@PLGA NP treatment by both administration methods. Similarly, K17 was demonstrated to be highly expressed in MET2 epidermis, especially in the invaded fronts, in the control and PLGA NP treated FTMs. However, both topical application and injection of DOX@PLGA NPs downregulated the expression of K17 in MET2-FTMs (Fig. 6J).

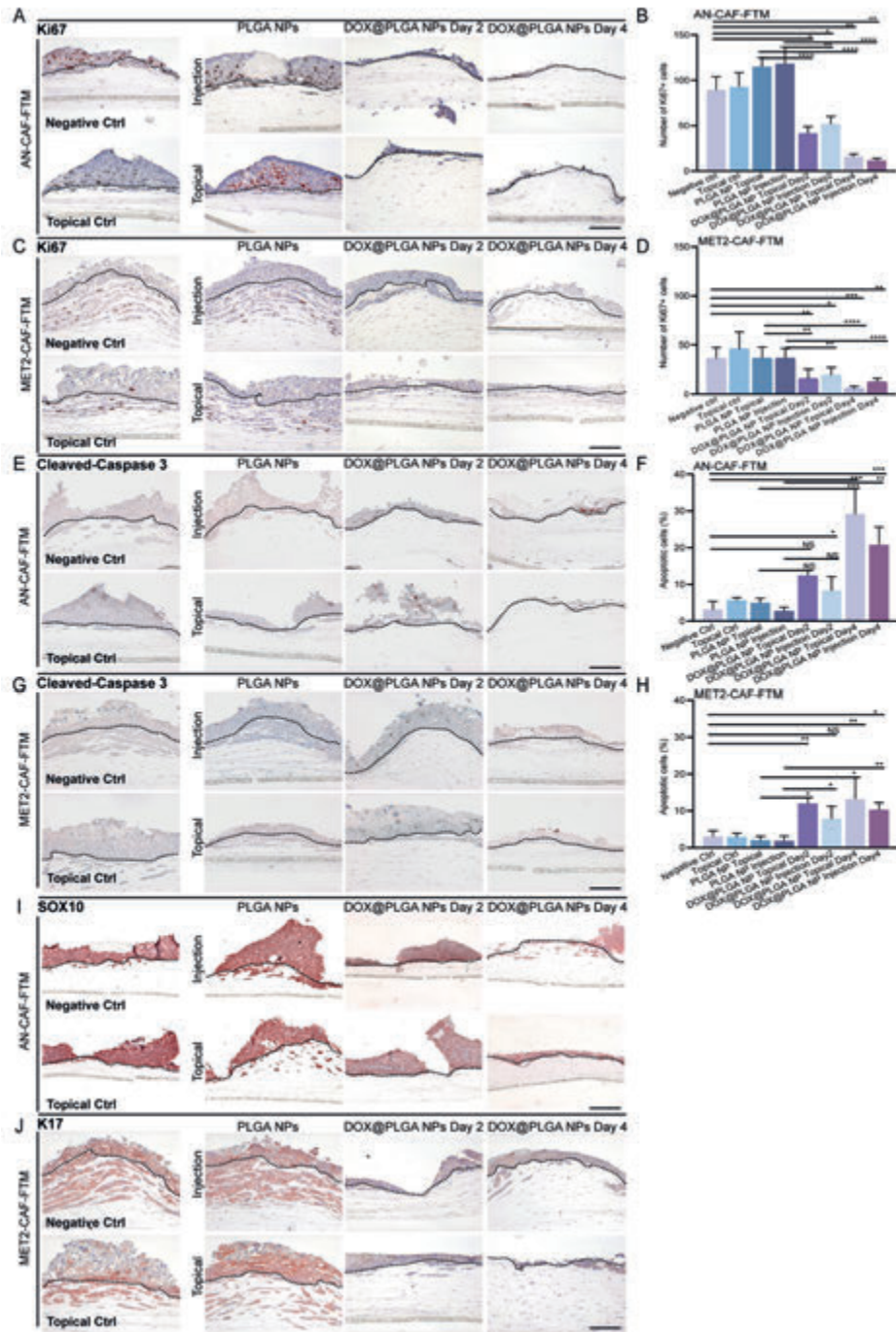


**Figure 6.** The anti-proliferative and pro-apoptotic effects of DOX@PLGA NPs in AN- and MET2-FITMs. (A) IHC staining of Ki67 in AN-FITMs. (C) IHC staining of

Ki67 in MET2-FTMs. (E) IHC staining of Cleaved Caspase 3 in AN-FTMs. (F) IHC staining of Cleaved Caspase 3 in AN-FTMs. (I) IHC staining of SOX10 in AN-FTMs. (J) IHC staining of K17 in MET2-FTMs. The number of Ki67 positive cells in (B) AN-FTMs, and (D) MET2-FTMs were calculated. Quantification of the percentage of Cleaved Caspase 3 positive tumor cells in all tumor cells in (F) AN-FTMs and (H) MET2-FTMs was performed. Scale bar = 100  $\mu$ m. Data was presented as mean  $\pm$  SD from 3 independent experiments. NS indicates  $p > 0.05$ , \*  $p < 0.05$ , \*\*  $p < 0.01$ , \*\*\*  $p < 0.001$ .

### 3.7 DOX@PLGA NPs attenuated CAF activation in SKCM and cSCC FTMs

Apart from the tumor cell-centered observations, we further explored if DOX@PLGA NPs could regulate CAFs simultaneously in 3D FTMs. To this end, we included two markers,  $\alpha$ -SMA and COL11A1, to assess CAFs activation [33]. As shown in Figure 7A–D, after interaction with AN or MET2 cells, CAFs remained their phenotype during the 3D co-culture by expressing  $\alpha$ -SMA robustly. PLGA NPs showed little effect on CAFs marker expression whereas treatment with DOX@PLGA NPs, especially by injection, led to a time-dependent decrease in the fluorescence intensity of  $\alpha$ -SMA. Topical treatment with DOX@PLGA NPs for 2 days did not significantly decrease the expression of  $\alpha$ -SMA, but a prolonged treatment for four days resulted in a noticeable decrease. For COL11A1 (Fig. 7E–H), we observed a similar expression pattern as  $\alpha$ -SMA in the dermal compartments in control and PLGA NP treatment groups in both AN- and MET2-FTMs. However, after 2 days of treatment with DOX@PLGA NPs, the expression of COL11A1 in the dermis was already significantly lower. When the treatment time was extended to 4 days, the protein expression of COL11A1 was not necessarily further downregulated.

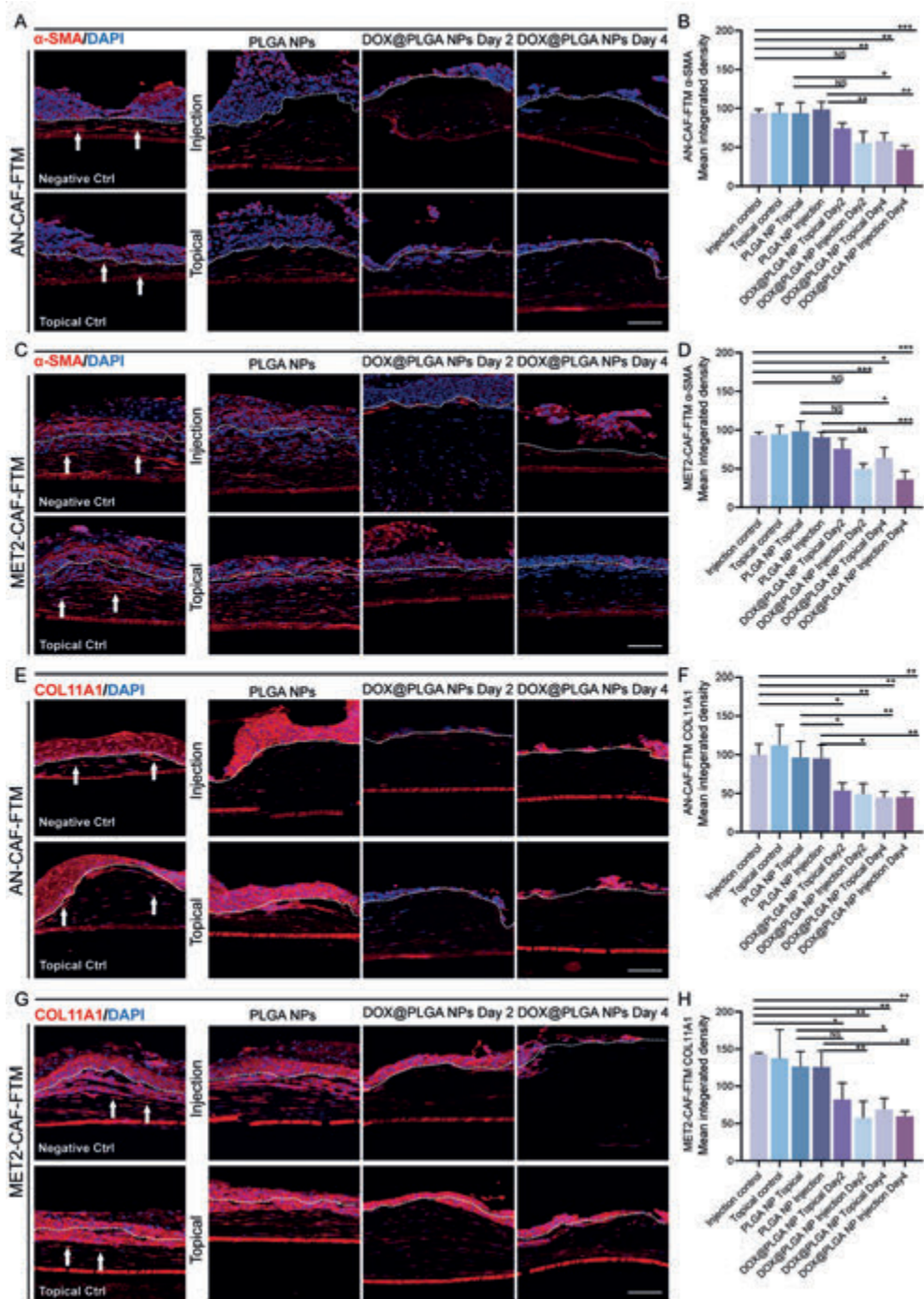


**Figure 7.** The effect of DOX@PLGA NPs on CAFs phenotype in AN- and MET2-FTMs. (A) Representative immunofluorescence staining of  $\alpha$ -SMA in AM-FTMs.

(B) Quantification of the Mean Integrated Density of  $\alpha$ -SMA in each AN-FTM. (C) Representative immunofluorescence staining of  $\alpha$ -SMA in MET2-FTMs. (D) Quantification of the Mean Integrated Density of  $\alpha$ -SMA in each MET2-FTM. (E) Representative immunofluorescence staining of COL11A1 in AM-FTMs. (F) Quantification of the Mean Integrated Density of COL11A1 in each AN-FTM. (G) Representative immunofluorescence staining of COL11A1 in MET2-FTMs. (H) Quantification of the Mean Integrated Density of COL11A1 in each MET2-FTM. Scale bar = 100  $\mu$ m. White arrows indicate positive staining in CAFs. Data was presented as mean  $\pm$  SD from 3 independent experiments. NS indicates  $p > 0.05$ , \*  $p < 0.05$ , \*\*  $p < 0.01$ , \*\*\*  $p < 0.001$ .

#### 4 Discussion

As a broad-spectrum chemotherapy drug, DOX was traditionally recognized as inhibiting the growth and proliferation of cancer cells by interfering with DNA replication and inducing DNA damage, which leads to apoptosis of cancer cells [34]. Existing research also indicates that DOX exerts anticancer effects through various other biological events, including the induction of tumor cell autophagy, senescence, and immunogenic cell death [35,36]. Although topical administration at the site of the skin tumor can reduce the systemic toxicity of DOX, this method can still cause skin irritation, inflammation, and even tissue necrosis. Moreover, DOX strongly interacts with the stratum corneum (SC), which greatly hinders its penetration into the skin [37,38]. Nanocarrier systems can be used to transport DOX through the SC barrier and accumulate in skin appendages, which have been demonstrated to act as reservoirs for nanoparticles, resulting in a sustained release of drugs in the epidermis [39,40]. Moreover, for early stages of skin cancer, lesions can be easily treated topically, thereby avoiding complications associated with systemic toxicity [41]. Several nanocarriers have been developed for DOX delivery, such as liposomes and polymeric NPs. PLGA is an FDA-approved polymer, and certain PLGA NP formulations are being utilized in clinical trials [36,42,43]. Furthermore, drugs encapsulated in PLGA NPs exhibit enhanced stability, particularly in body fluids, in comparison to other colloidal delivery systems or free drugs [33,34]. Therefore, in this study, we synthesized DOX-loaded PLGA NPs (DOX@PLGA NPs) and explored their potential for treating SKCM and cSCC.

The detection results of nanoparticle size in this study indicate that the addition of DOX reduces the particle size of the nanoparticles. We believe this is related to the characteristics of DOX, its concentration, and its miscibility with the polymer. As previously reported, DOX, a hydrophobic drug, may decrease the overall

hydrophilicity of the polymer matrix. The incorporation of DOX may alter the self-assembly ability of PLGA, resulting in a tighter structure and a reduction in nanoparticle size [44,45]. Higher drug concentrations lead to stronger interactions between the drug and the polymer, resulting in higher encapsulation efficiency and smaller particle size [46,47]. DOX and PLGA may exhibit a certain degree of miscibility, which enhanced miscibility can facilitate the formation of more homogeneous and compact nanoparticles, contributing to a reduction in particle size [48].

In line with other studies, DOX@PLGA NPs showed great anti-proliferative and pro-apoptotic effects in SKCM and cSCC cell lines. Compared to the  $IC_{50}$  of DOX-loaded polymeric NPs in other cell lines from breast cancer [49,50], lung cancer [51], and hepatocellular carcinoma [52], our results showed that DOX@PLGA NPs induced > 50% cell death within 48 h in SKCM and cSCC cell lines at a relatively lower concentration of loaded DOX (below 1  $\mu\text{g}/\text{mL}$ ). This suggests that SKCM and cSCC cell lines are highly sensitive to DOX@PLGA NPs. Aside from the effects on tumor cells, the effect of DOX on CAFs has not been investigated yet. In this study, we found out that DOX@PLGA NPs inhibited CAF cell survival in a time- and dosage-dependent manner. However, under the same conditions, the  $IC_{50}$  of DOX@PLGA NPs in CAFs was almost 4 times higher than in tumor cells. The fact that CAFs have better survival rates when exposed to DOX compared to tumor cells might partially explain why CAFs are important contributors to chemotherapy resistance in cancer therapy [6], as the majority of CAFs would remain and keep nurturing the survived tumor cells. Therefore this provides a theoretical basis for future DOX-loaded NP therapies in which multi-targeting strategies using different concentrations of drugs should be prioritized. Next, we further explored the effect of DOX@PLGA NPs on CAF marker expression.  $\alpha$ -SMA is identified as one of the most frequently used CAF markers [53]. The presence of  $\alpha$ -SMA-positive CAFs released tumor-promoting growth factors and cytokines, enhanced tissue contractility to facilitate ECM remodeling and were associated with poor prognosis in various carcinomas [54,55]. COL11A1 is a newly identified CAF marker commonly not expressed in stroma cells in healthy tissues, benign fibrotic or inflammatory pathological processes, whereas rich in the stroma of various carcinomas [56–58]. Moreover, CAF-secreted VCAM-1 was shown to enhance growth and invasion by activating the AKT and MAPK signaling pathways in lung cancer cells and positively correlates with  $\alpha$ -SMA expression [27]. In our study, DOX@PLGA NPs significantly downregulated the expression of up-mentioned markers, especially COL11A1, indicating the potential of DOX@PLGA NPs as TME-targeted therapy. This is rather exciting since, to date, very limited amount of studies have focused on using NP to target CAFs [59]. The mechanism of

how DOX@PLGA NPs regulate CAFs functions and phenotypes awaits further investigations. Additionally, the TME is usually acidic compared to normal physiological environments. The DOX release went from around 70% in pH at 7.4 to 90% in pH at 5.0 after 48 h which again indicates the proper strength of using PLGA NPs in cancer therapy.

To mimic the tumor-stroma interactions that occur in solid tumors, we established 3D SKCM and cSCC tumor FTMs consisting of a stratified tumorous epidermis with a dermis populated with CAFs. CAFs in these models clearly induced tumor cell proliferation and invasion judged by the histological analysis and the expression of Ki67, which was significantly suppressed by DOX@PLGA NPs treatment. Moreover, DOX@PLGA NPs significantly elevated C-C3 expression in both SKCM and cSCC FTMs, and the longer the treatment time, the higher the apoptosis rate of cancer cells becomes. Consistent with the findings in our 2D cell line study, these results suggested that DOX@PLGA NPs possess promising anti-proliferative and pro-apoptotic effects on SKCM and cSCC cells. Inhibiting the aggressiveness of tumor cells is also crucial in the treatment of malignant tumors. For instance, SOX10 is often used as a metastasis marker in malignant melanoma, and the number of SOX-10-positive melanoma cells is indicative of the aggressiveness of melanoma cells [60,61]. In our study, we found that the expression level of SOX10 decreased after treatment of AN-CAF-FTM with DOX@PLGA NPs, suggesting that DOX@PLGA NPs can effectively inhibit the invasiveness of AN cells. In addition, DOX@PLGA NPs effectively reduced k17 expression in MET2 cells in 3D cSCC models. K17 expression is usually absent in normal epidermis, whereas in epithelial cells undergoing hyperproliferation or abnormal differentiation (e.g., wound healing), its expression is upregulated [32,62]. It has been reported that K17 expression level closely correlates with cancer metastasis, suggesting that K17 has potential as a diagnostic and prognostic biomarker in multiple types of carcinomas [63]. The sharp decrease of K17 expression after treatment with DOX@PLGA NPs indicated a less-aggressive state of keratinocytes in MET2-FTMs.

As tumor stroma is an integral part of cancer progression, we simultaneously investigated the effect of DOX@PLGA NPs on CAFs in FTMs. CAFs expressed a consistently high level of  $\alpha$ -SMA and COL11A1 expression after interacting with AN and MET2 cells, indicating that the CAF phenotype was maintained in these tumorous FTMs, which might partially explain the observed tumor invasive behavior in both control and PLGA NP treated CAF-FTMs. Consistent with our 2D results, the expression of  $\alpha$ -SMA and COL11A1 was significantly reduced after treatment with DOX@PLGA NPs in both AN- and MET2-FTMs. Interestingly, COL11A1 intensity was significantly decreased after 2 days of topical treatment

compared to  $\alpha$ -SMA, indicating that COL11A1 might be more sensitive to DOX@PLGA NP treatment. This finding was consistent with our monolayer observation, which showed that the COL11A1 mRNA expression in CAFs was 20 times lower after treatment with DOX@PLGA NPs compared to the control. Since COL11A1 is synthesized and secreted from CAFs, and eventually deposited in the ECM during tumor progression, DOX@PLGA NPs might play an important role in remodeling the position of ECM components, which requires further investigations. However, the use of  $\alpha$ -SMA as a specific CAF marker is also limited due to its low expression in inflammatory CAFs [64]. COL11A1 has great potential for CAF identification, but further in-depth studies are required for universal acknowledgement. In fact, one of the obstacles in current CAF-targeting therapy is the heterogeneity and functional diversity of CAFs. To fully unravel the applicability and regulatory effect of DOX@PLGA NPs on CAFs, more specific CAF markers should be included in future studies.

*In vitro* 3D skin equivalents including FTM were developed since 1948 and substantially improved over the past years in our research group to closely mimic the morphology and barrier function of the native skin [15]. Furthermore, we included topical application and intradermal injection as the treatment methods in this study, as these are the two universally used drug administration methods in the dermatological field. Luengo *et al.* once demonstrated that PLGA NPs could enhance the permeation of flufenamic acid in epidermis by the pH decrease during polymer hydrolytic degradation [65]. In line with this study, we observed obvious accumulation of NPs within the tumor epidermis and effective penetration through the epidermis to the dermis after topical treatment, indicating the potential of topical administration of PLGA NPs. This observation was further strengthened by the decrease of CAF marker expression as previously mentioned. However, the topical administration has its own limitation since we noticed that mainly CAFs in the upper layer of dermis were affected, indicating limited penetration ability of DOX@PLGA NPs on FTMs. Future studies should also cover the topic of optimization or modification of PLGA NPs to achieve better penetration of the skin. Meanwhile, intradermal injection of DOX@PLGA NPs had less effect on inducing apoptosis in tumor epidermis but stronger downregulation of CAF marker expression compared to topical treatment, which is reasonable because the primary target of this method is CAFs themselves. Noticeably, unlike the topical treatment, less accumulation of NPs was observed in the dermis in the injection group. By using a syringe for injection treatment, the precision of release control is challenged. Microneedles might be a good solution for more precise injection. Nevertheless, as this type of work has never been done before, we expect room for optimizations.

## 5 Conclusions

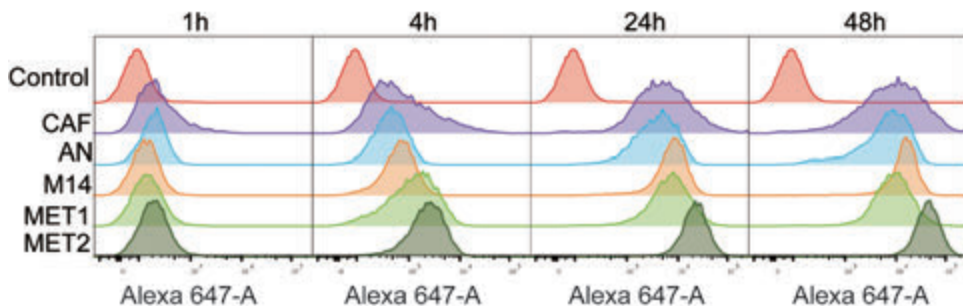
This is the first study to show the applicability of DOX-loaded PLGA nano-delivery system in 3D SKCM and cSCC FTMs, which exhibit improved characteristics of human skin structure as well as facilitate the understanding of the crosstalk between tumor cells and the TME. DOX@PLGA NPs can effectively deliver into tumor cells, inhibit tumor cell growth, promote apoptosis, demonstrate promising uptake ability in CAFs, and lead to the de-activation of CAFs. These results revealed the potency of utilizing *in vitro* 3D skin models as a platform for nanocarrier-related studies in skin cancers, and suggested new effects of DOX-loaded PLGA NPs on CAFs, which brings new insights for TME-targeting therapy.

Supplementary Materials:

**Supplementary Table 1.** qPCR primers

Gene/h	Forward primer 5' > 3'	Reverse primer 5' > 3'
Gene of interest		
VCAM	CAGGCTGGAAGAAGCAGAAAG	TGTCTCCTTCTTTGACACTCTCAG
$\alpha$ -SMA	CTCGGGCTGAAGAAGGAACCCAA	ATTGGCACACGGCAGGTGGT
COL11A1	AAAGCACTTCGCTTCTCTGGG	GACAGTCTTTTCATAGCCTTTTCTG
Reference Gene		
SDHA	AACCAAACGCTGGGGAAGAA	GGAACACGGCAGCATGATT
TBP	GAATATGGTGGGAGCTGTGA	AAACCAGGAAATAACTCTGGCTCA
HPRT	TTGCTTTCCTTGGTCAGGCA	ATCCAACACTTCGTGGGGTC

**Supplementary Figure 1.**



After incubating AN, M14, MET1, MET2 and CAFs cells with or without PLGA NPs for 0, 1, 24, and 48 h, cells were collected for flow cytometry. Representative flow cytograms of the uptake of DID-labeled PLGA NPs in each cell type were presented.

## References

1. Perez, M.; Abisaad, J.A.; Rojas, K.D.; Marchetti, M.A.; Jaimes, N. Skin cancer: Primary, secondary, and tertiary prevention. Part I. *J Am Acad Dermatol* 2022, 87, 255-268, doi:10.1016/j.jaad.2021.12.066.
2. Que, S.K.T.; Zwald, F.O.; Schmults, C.D. Cutaneous squamous cell carcinoma: Incidence, risk factors, diagnosis, and staging. *J Am Acad Dermatol* 2018, 78, 237-247, doi:10.1016/j.jaad.2017.08.059.
3. Mao, X.; Xu, J.; Wang, W.; Liang, C.; Hua, J.; Liu, J.; Zhang, B.; Meng, Q.; Yu, X.; Shi, S. Crosstalk between cancer-associated fibroblasts and immune cells in the tumor microenvironment: New findings and future perspectives. *Molecular cancer* 2021, 20, 1-30.
4. Aronovich, A.; Moyal, L.; Gorovitz, B.; Amitay-Laish, I.; Naveh, H.P.; Forer, Y.; Maron, L.; Knaneh, J.; Ad-El, D.; Yaacobi, D., et al. Cancer-Associated Fibroblasts in Mycosis Fungoides Promote Tumor Cell Migration and Drug Resistance through Cxcl12/CXCR4. *J Invest Dermatol* 2021, 141, 619-627. e612, doi:10.1016/j.jid.2020.06.034.
5. Hirata, E.; Girotti, M.R.; Viros, A.; Hooper, S.; Spencer-Dene, B.; Matsuda, M.; Larkin, J.; Marais, R.; Sahai, E. Intravital imaging reveals how BRAF inhibition generates drug-tolerant microenvironments with high integrin  $\beta$ 1/FAK signaling. *Cancer Cell* 2015, 27, 574-588, doi:10.1016/j.ccell.2015.03.008.
6. Saw, P.E.; Chen, J.; Song, E. Targeting CAFs to overcome anticancer therapeutic resistance. *Trends Cancer* 2022, 8, 527-555, doi:10.1016/j.trecan.2022.03.001.
7. Begines, B.; Ortiz, T.; Perez-Aranda, M.; Martinez, G.; Merinero, M.; Arguelles-Arias, F.; Alcudia, A. Polymeric Nanoparticles for Drug Delivery: Recent Developments and Future Prospects. *Nanomaterials (Basel)* 2020, 10, doi:10.3390/nano10071403.
8. Félix Lanao, R.P.; Jonker, A.M.; Wolke, J.G.; Jansen, J.A.; van Hest, J.C.; Leeuwenburgh, S.C. Physicochemical properties and applications of poly (lactic-co-glycolic acid) for use in bone regeneration. *Tissue Eng Part B Rev* 2013, 19, 380-390, doi:10.1089/ten.TEB.2012.0443.
9. Operti, M.C.; Bernhardt, A.; Grimm, S.; Engel, A.; Figdor, C.G.; Tagit, O. PLGA-based nanomedicines manufacturing: Technologies overview and challenges in industrial scale-up. *Int J Pharm* 2021, 605, 120807, doi:10.1016/j.ijpharm.2021.120807.

10. De, R.; Mahata, M.K.; Kim, K.T. Structure-Based Varieties of Polymeric Nanocarriers and Influences of Their Physicochemical Properties on Drug Delivery Profiles. *Adv Sci (Weinh)* 2022, 9, e2105373, doi:10.1002/adv.202105373.
11. Rezvantalab, S.; Drude, N.I.; Moraveji, M.K.; Güvener, N.; Koons, E.K.; Shi, Y.; Lammers, T.; Kiessling, F. PLGA-Based Nanoparticles in Cancer Treatment. *Front Pharmacol* 2018, 9, 1260, doi:10.3389/fphar.2018.01260.
12. Galluzzi, L.; Vitale, I.; Warren, S.; Adjemian, S.; Agostinis, P.; Martinez, A.B.; Chan, T.A.; Coukos, G.; Demaria, S.; Deutsch, E., et al. Consensus guidelines for the definition, detection and interpretation of immunogenic cell death. *J Immunother Cancer* 2020, 8, doi:10.1136/jitc-2019-000337.
13. Fritz P. Schmook, J.G.M., Andreas Billich \*. Comparison of human skin or epidermis models with human and animal skin in in-vitro percutaneous absorption. *International Journal of Pharmaceutics* 2001, 215, 51-56, doi:10.1016/s0378-5173 (00)00665-7.
14. Walters, K.A.; Watkinson, A.C.; Brain, K.R. In vitro skin permeation evaluation: the only realistic option. *Int J Cosmet Sci* 1998, 20, 307-316, doi:10.1046/j.1467-2494.1998.181622.x.
15. Bouwstra, J.A.; Helder, R.W.J.; El Ghalbzouri, A. Human skin equivalents: Impaired barrier function in relation to the lipid and protein properties of the stratum corneum. *Adv Drug Deliv Rev* 2021, 175, 113802, doi:10.1016/j.addr.2021.05.012.
16. Maksimenko, O.; Malinovskaya, J.; Shipulo, E.; Osipova, N.; Razzhivina, V.; Arantseva, D.; Yarovaya, O.; Mostovaya, U.; Khalansky, A.; Fedoseeva, V., et al. Doxorubicin-loaded PLGA nanoparticles for the chemotherapy of glioblastoma: Towards the pharmaceutical development. *Int J Pharm* 2019, 572, 118733, doi:10.1016/j.ijpharm.2019.118733.
17. Risnayanti, C.; Jang, Y.S.; Lee, J.; Ahn, H.J. PLGA nanoparticles co-delivering Mdr1 and BCL2 siRNA for overcoming resistance of paclitaxel and cisplatin in recurrent or advanced ovarian cancer. *Sci Rep* 2018, 8, 7498, doi:10.1038/s41598-018-25930-7.
18. Tsai, L.H.; Yen, C.H.; Hsieh, H.Y.; Young, T.H. Doxorubicin Loaded PLGA Nanoparticle with Cationic/Anionic Polyelectrolyte Decoration: Characterization, and Its Therapeutic Potency. *Polymers (Basel)* 2021, 13, doi:10.3390/polym13050693.
19. Issa Amjadia, M.R.a.M.-S.H., b\*. Anticancer Activity of Nanoparticles

Based on PLGA and its Co-polymer: Invitro Evaluation. Iranian Journal of Pharmaceutical Research 2013.

20. Cruz, L.J.; van Dijk, T.; Vepris, O.; Li, T.; Schomann, T.; Baldazzi, F.; Kurita, R.; Nakamura, Y.; Grosveld, F.; Philippsen, S., et al. PLGA-Nanoparticles for Intracellular Delivery of the CRISPR-Complex to Elevate Fetal Globin Expression in Erythroid Cells. *Biomaterials* 2021, 268, 120580, doi:10.1016/j.biomaterials.2020.120580.
21. Ahmed, M.M.; Fatima, F.; Anwer, M.K.; Aldawsari, M.F.; Bhatia, S.; Al-Harrasi, A. Brigatinib loaded poly (d,l-lactide-co-glycolide) nanoparticles for improved anti-tumoral activity against non-small cell lung cancer cell lines. *Drug Dev Ind Pharm* 2021, 47, 1112-1120, doi:10.1080/03639045.2021.1983585.
22. Moore, T.L.; Rodriguez-Lorenzo, L.; Hirsch, V.; Balog, S.; Urban, D.; Jud, C.; Rothen-Rutishauser, B.; Lattuada, M.; Petri-Fink, A. Nanoparticle colloidal stability in cell culture media and impact on cellular interactions. *Chem Soc Rev* 2015, 44, 6287-6305, doi:10.1039/c4cs00487f.
23. Palanikumar, L.; Al-Hosani, S.; Kalmouni, M.; Nguyen, V.P.; Ali, L.; Pasricha, R.; Barrera, F.N.; Magzoub, M. pH-responsive high stability polymeric nanoparticles for targeted delivery of anticancer therapeutics. *Commun Biol* 2020, 3, 95, doi:10.1038/s42003-020-0817-4.
24. Wan, S.; Zhang, L.; Quan, Y.; Wei, K. Resveratrol-loaded PLGA nanoparticles: enhanced stability, solubility and bioactivity of resveratrol for non-alcoholic fatty liver disease therapy. *R Soc Open Sci* 2018, 5, 181457, doi:10.1098/rsos.181457.
25. Edlich, F. BCL-2 proteins and apoptosis: Recent insights and unknowns. *Biochem Biophys Res Commun* 2018, 500, 26-34, doi:10.1016/j.bbrc.2017.06.190.
26. Wu, Y.H.; Huang, Y.F.; Chang, T.H.; Chen, C.C.; Wu, P.Y.; Huang, S.C.; Chou, C.Y. COL11A1 activates cancer-associated fibroblasts by modulating TGF- $\beta$ 3 through the NF- $\kappa$ B/IGFBP2 axis in ovarian cancer cells. *Oncogene* 2021, 40, 4503-4519, doi:10.1038/s41388-021-01865-8.
27. Zhou, Z.; Zhou, Q.; Wu, X.; Xu, S.; Hu, X.; Tao, X.; Li, B.; Peng, J.; Li, D.; Shen, L., et al. VCAM-1 secreted from cancer-associated fibroblasts enhances the growth and invasion of lung cancer cells through AKT and MAPK signaling. *Cancer Lett* 2020, 473, 62-73, doi:10.1016/j.canlet.2019.12.039.
28. Yoshida, G.J. Regulation of heterogeneous cancer-associated fibroblasts: the molecular pathology of activated signaling pathways. *J Exp Clin Cancer Res* 2020, 39, 112, doi:10.1186/s13046-020-01611-0.

29. Liu, P.F.; Hu, Y.C.; Kang, B.H.; Tseng, Y.K.; Wu, P.C.; Liang, C.C.; Hou, Y.Y.; Fu, T.Y.; Liou, H.H.; Hsieh, I.C., et al. Expression levels of cleaved caspase-3 and caspase-3 in tumorigenesis and prognosis of oral tongue squamous cell carcinoma. *PLoS One* 2017, 12, e0180620, doi:10.1371/journal.pone.0180620.
30. Waster, P.; Eriksson, I.; Vainikka, L.; Rosdahl, I.; Ollinger, K. Extracellular vesicles are transferred from melanocytes to keratinocytes after UVA irradiation. *Sci Rep* 2016, 6, 27890, doi:10.1038/srep27890.
31. Capparelli, C.; Purwin, T.J.; Glasheen, M.; Caksa, S.; Tiago, M.; Wilski, N.; Pomante, D.; Rosenbaum, S.; Nguyen, M.Q.; Cai, W., et al. Targeting SOX10-deficient cells to reduce the dormant-invasive phenotype state in melanoma. *Nat Commun* 2022, 13, 1381, doi:10.1038/s41467-022-28801-y.
32. Zeng, Y.; Zou, M.; Liu, Y.; Que, K.; Wang, Y.; Liu, C.; Gong, J.; You, Y. Keratin 17 Suppresses Cell Proliferation and Epithelial-Mesenchymal Transition in Pancreatic Cancer. *Front Med (Lausanne)* 2020, 7, 572494, doi:10.3389/fmed.2020.572494.
33. Nurmik, M.; Ullmann, P.; Rodriguez, F.; Haan, S.; Letellier, E. In search of definitions: Cancer-associated fibroblasts and their markers. *Int J Cancer* 2020, 146, 895-905, doi:10.1002/ijc.32193.
34. Mohan, P.; Rapoport, N. Doxorubicin as a molecular nanotheranostic agent: effect of doxorubicin encapsulation in micelles or nanoemulsions on the ultrasound-mediated intracellular delivery and nuclear trafficking. *Mol Pharm* 2010, 7, 1959-1973, doi:10.1021/mp100269f.
35. He, Y.; de Araújo Júnior, R.F.; Cavalcante, R.S.; Yu, Z.; Schomann, T.; Gu, Z.; Eich, C.; Cruz, L.J. Effective breast cancer therapy based on palmitic acid-loaded PLGA nanoparticles. *Biomaterials Advances* 2023, 145, doi:10.1016/j.bioadv.2022.213270.
36. Vasey, P.A.; Kaye, S.B.; Morrison, R.; Twelves, C.; Wilson, P.; Duncan, R.; Thomson, A.H.; Murray, L.S.; Hilditch, T.E.; Murray, T., et al. Phase I clinical and pharmacokinetic study of PK1 [N-(2-hydroxypropyl)methacrylamide copolymer doxorubicin]: first member of a new class of chemotherapeutic agents-drug-polymer conjugates. Cancer Research Campaign Phase I/II Committee. *Clin Cancer Res* 1999, 5, 83-94.
37. Herai, H.; Gratieri, T.; Thomazine, J.A.; Bentley, M.V.; Lopez, R.F. Doxorubicin skin penetration from monoolein-containing propylene glycol formulations. *Int J Pharm* 2007, 329, 88-93, doi:10.1016/j.ijpharm.2006.08.021.

38. Taveira, S.F.; Nomizo, A.; Lopez, R.F. Effect of the iontophoresis of a chitosan gel on doxorubicin skin penetration and cytotoxicity. *J Control Release* 2009, 134, 35-40, doi:10.1016/j.jconrel.2008.11.002.
39. Qu, F.; Geng, R.; Liu, Y.; Zhu, J. Advanced nanocarrier- and microneedle-based transdermal drug delivery strategies for skin diseases treatment. *Theranostics* 2022, 12, 3372-3406, doi:10.7150/thno.69999.
40. Pandey, M.; Choudhury, H.; Gorain, B.; Tiong, S.Q.; Wong, G.Y.S.; Chan, K.X.; They, X.; Chieu, W.S. Site-Specific Vesicular Drug Delivery System for Skin Cancer: A Novel Approach for Targeting. *Gels* 2021, 7, doi:10.3390/gels7040218.
41. Zeng, L.; Gowda, B.H.J.; Ahmed, M.G.; Abourehab, M.A.S.; Chen, Z.S.; Zhang, C.; Li, J.; Kesharwani, P. Advancements in nanoparticle-based treatment approaches for skin cancer therapy. *Mol Cancer* 2023, 22, 10, doi:10.1186/s12943-022-01708-4.
42. Schütz, C.A.; Juillerat-Jeanneret, L.; Mueller, H.; Lynch, I.; Riediker, M. Therapeutic nanoparticles in clinics and under clinical evaluation. *Nanomedicine (Lond)* 2013, 8, 449-467, doi:10.2217/nnm.13.8.
43. Barenholz, Y. Doxil®--the first FDA-approved nano-drug: lessons learned. *J Control Release* 2012, 160, 117-134, doi:10.1016/j.jconrel.2012.03.020.
44. Hickey, J.W.; Santos, J.L.; Williford, J.M.; Mao, H.Q. Control of polymeric nanoparticle size to improve therapeutic delivery. *J Control Release* 2015, 219, 536-547, doi:10.1016/j.jconrel.2015.10.006.
45. Dashtimoghadam, E.; Mirzadeh, H.; Taromi, F.A.; Nyström, B. Microfluidic self-assembly of polymeric nanoparticles with tunable compactness for controlled drug delivery. *Polymer* 2013, 54, 4972-4979, doi:https://doi.org/10.1016/j.polymer.2013.07.022.
46. Song, X.; Zhao, Y.; Hou, S.; Xu, F.; Zhao, R.; He, J.; Cai, Z.; Li, Y.; Chen, Q. Dual agents loaded PLGA nanoparticles: systematic study of particle size and drug entrapment efficiency. *Eur J Pharm Biopharm* 2008, 69, 445-453, doi:10.1016/j.ejpb.2008.01.013.
47. Lu, Y.; Chowdhury, D.; Vladisavljević, G.T.; Koutroumanis, K.; Georgiadou, S. Production of Fluconazole-Loaded Polymeric Micelles Using Membrane and Microfluidic Dispersion Devices. *Membranes (Basel)* 2016, 6, doi:10.3390/membranes6020029.
48. Abioye, A.O.; Chi, G.T.; Kola-Mustapha, A.T.; Ruparelia, K.C.; Beresford, K.J.M.; Arroo, R.R.J. Polymer-drug nanoconjugate – an innovative

- nanomedicine: challenges and recent advancements in rational formulation design for effective delivery of poorly soluble drugs. pp. 38 - 79.
49. He, Y.; de Araújo Júnior, R.F.; Cavalcante, R.S.; Yu, Z.; Schomann, T.; Gu, Z.; Eich, C.; Cruz, L.J. Effective breast cancer therapy based on palmitic acid-loaded PLGA nanoparticles. *Biomater Adv* 2023, 145, 213270, doi:10.1016/j.bioadv.2022.213270.
  50. Misiak, P.; Niemirowicz-Laskowska, K.; Markiewicz, K.H.; Wielgat, P.; Kurowska, I.; Czarnomysy, R.; Misztalewska-Turkowicz, I.; Car, H.; Bielawski, K.; Wilczewska, A.Z. Doxorubicin-loaded polymeric nanoparticles containing ketoester-based block and cholesterol moiety as specific vehicles to fight estrogen-dependent breast cancer. *Cancer Nanotechnology* 2023, 14, doi:10.1186/s12645-023-00176-9.
  51. Zhang, J.; Tao, W.; Chen, Y.; Chang, D.; Wang, T.; Zhang, X.; Mei, L.; Zeng, X.; Huang, L. Doxorubicin-loaded star-shaped copolymer PLGA-vitamin E TPGS nanoparticles for lung cancer therapy. *J Mater Sci Mater Med* 2015, 26, 165, doi:10.1007/s10856-015-5498-z.
  52. Kuruvilla, S.P.; Tiruchinapally, G.; Crouch, A.C.; ElSayed, M.E.H.; Greve, J.M. Dendrimer-doxorubicin conjugates exhibit improved anticancer activity and reduce doxorubicin-induced cardiotoxicity in a murine hepatocellular carcinoma model. *PLoS One* 2017, 12, e0181944, doi:10.1371/journal.pone.0181944.
  53. Mezawa, Y.; Orimo, A. The roles of tumor- and metastasis-promoting carcinoma-associated fibroblasts in human carcinomas. *Cell Tissue Res* 2016, 365, 675-689, doi:10.1007/s00441-016-2471-1.
  54. Yamashita, M.; Ogawa, T.; Zhang, X.; Hanamura, N.; Kashikura, Y.; Takamura, M.; Yoneda, M.; Shiraishi, T. Role of stromal myofibroblasts in invasive breast cancer: stromal expression of alpha-smooth muscle actin correlates with worse clinical outcome. *Breast Cancer* 2012, 19, 170-176, doi:10.1007/s12282-010-0234-5.
  55. Maeshima, A.M.; Niki, T.; Maeshima, A.; Yamada, T.; Kondo, H.; Matsuno, Y. Modified scar grade: a prognostic indicator in small peripheral lung adenocarcinoma. *Cancer* 2002, 95, 2546-2554, doi:10.1002/cncr.11006.
  56. Fuentes-Martínez, N.; García-Pravia, C.; García-Ocaña, M.; Menéndez-Rodríguez, P.; Del Amo, J.; Suárez-Fernández, L.; Galván, J.A.; De los Toyos, J.R.; Barneo, L. Overexpression of proCOL11A1 as a stromal marker of breast cancer. *Histol Histopathol* 2015, 30, 87-93, doi:10.14670/hh-30.87.

57. Erkan, M.; Weis, N.; Pan, Z.; Schwager, C.; Samkharadze, T.; Jiang, X.; Wirkner, U.; Giese, N.A.; Ansorge, W.; Debus, J., et al. Organ-, inflammation- and cancer specific transcriptional fingerprints of pancreatic and hepatic stellate cells. *Mol Cancer* 2010, 9, 88, doi:10.1186/1476-4598-9-88.
58. Vázquez-Villa, F.; García-Ocaña, M.; Galván, J.A.; García-Martínez, J.; García-Pravia, C.; Menéndez-Rodríguez, P.; González-del Rey, C.; Barneo-Serra, L.; de Los Toyos, J.R. COL11A1/ (pro)collagen 11A1 expression is a remarkable biomarker of human invasive carcinoma-associated stromal cells and carcinoma progression. *Tumour Biol* 2015, 36, 2213-2222, doi:10.1007/s13277-015-3295-4.
59. Yang, M.; Li, J.; Gu, P.; Fan, X. The application of nanoparticles in cancer immunotherapy: Targeting tumor microenvironment. *Bioact Mater* 2021, 6, 1973-1987, doi:10.1016/j.bioactmat.2020.12.010.
60. Szumera-Ciećkiewicz, A.; Bosisio, F.; Teterycz, P.; Antoranz, A.; Delogu, F.; Koljenović, S.; van de Wiel, B.A.; Blokk, W.; van Kempen, L.C.; Rutkowski, P. SOX10 is as specific as S100 protein in detecting metastases of melanoma in lymph nodes and is recommended for sentinel lymph node assessment. *European Journal of Cancer* 2020, 137, 175-182.
61. Pytlak, B.; Prochorec-Sobieszek, M.; Szumera-Ciećkiewicz, A. SOX10 as an immunohistochemical marker in cancer diagnostics. *Biuletyn Polskiego Towarzystwa Onkologicznego Nowotwory* 2019, 4, 72-78.
62. Liesbeth Hameetman<sup>1</sup>, Suzan Commandeur<sup>2</sup>, Jan Nico Bouwes Bavinck<sup>2</sup>, Hermina C Wisgerhof<sup>2</sup>, Frank R de Gruijl<sup>2</sup>, Rein Willemze<sup>2</sup>, Leon Mullenders<sup>1</sup>, Cornelis P Tensen<sup>2\*</sup> and Harry Vrieling<sup>1\*</sup>. Molecular profiling of cutaneous squamous cell carcinomas and actinic keratoses from organ transplant recipients. *BMC Cancer* 2013, 13, 1-16, doi:doi:10.1186/1471-2407-13-58.
63. Yang, L.; Zhang, S.; Wang, G. Keratin 17 in disease pathogenesis: from cancer to dermatoses. *J Pathol* 2019, 247, 158-165, doi:10.1002/path.5178.
64. Öhlund, D.; Handly-Santana, A.; Biffi, G.; Elyada, E.; Almeida, A.S.; Ponz-Sarvisé, M.; Corbo, V.; Oni, T.E.; Hearn, S.A.; Lee, E.J., et al. Distinct populations of inflammatory fibroblasts and myofibroblasts in pancreatic cancer. *J Exp Med* 2017, 214, 579-596, doi:10.1084/jem.20162024.
65. Luengo, J.; Schneider, M.; Schneider, A.M.; Lehr, C.M.; Schaefer, U.F. Human Skin Permeation Enhancement Using PLGA Nanoparticles Is Mediated by Local pH Changes. *Pharmaceutics* 2021, 13, doi:10.3390/pharmaceutics13101608.